

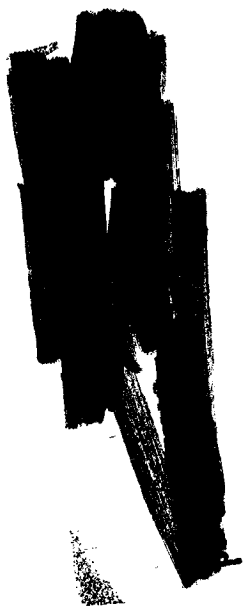
GPO PRICE \$ \_\_\_\_\_

CFSTI PRICE(S) \$ \_\_\_\_\_

Hard copy (HC) \$2,00

Microfiche (MF) 150

ff 653 July 65



RÉSUMÉ OF RECENT PARAWING RESEARCH

By Francis M. Rogallo, William C. Sleeman, Jr.,  
and Delwin R. Croom

NASA Langley Research Center  
Langley Station, Hampton, Va.

Presented at the Course on Aerodynamic Deceleration  
at the Center for Continuation Study, University of Minnesota

FACILITY FORM 602

**N66 27074**

(ACCESSION NUMBER)

(THRU)

**38**

(PAGES)

(CODE)

**TMX-56747**

(NASA CR OR TMX OR AD NUMBER)

**01**

(CATEGORY)

Minneapolis, Minnesota  
July 8, 1965

## RÉSUMÉ OF RECENT PARAWING RESEARCH

By Francis M. Rogallo, William C. Sleeman, Jr.,  
and Delwin R. Croom

NASA Langley Research Center

### INTRODUCTION

Many research investigations of flexible wings (paragliders, parawings) have been conducted by the National Aeronautics and Space Administration in the past several years. This work has been concerned with many different types of parawing configurations and one of the purposes of this paper is to show how these separate investigations are related and how each type of configuration fits into the overall spectrum of aeroflexible lifting surfaces. Some recent experimental results on wings of current interest will be reviewed; some important problem areas and some possible design trade-offs will be discussed. The most recent parawing work being conducted at the Langley Research Center is on the completely flexible-limp paraglider (wing-type gliding parachute) and a summary of these test results which were obtained in the 17-foot test section of the Langley 300 mph 7- by 10-foot tunnel is presented.

A combined list of references and a bibliography of parawing publications is given at the end of the text.

### OVERALL SPECTRUM OF PARAWINGS

Figure 1 presents the spectrum of parawing configurations and the maximum lift-drag ratios obtained in NASA wind-tunnel tests of each type of wing shown. The lower end of the spectrum, indicated as having no structure, represents the original concept of a flexible lifting surface. The shaded area labeled limp paraglider indicates that this type of lifting surface can provide maximum lift-drag ratios up to about 3. The use of some structural stiffness such as would be obtained with a single-curvature lifting surface made of flexible, thin sheet metal or plastic provided maximum lift-drag ratios of around 6.

### Conical Wings

Early flight tests at the Langley Research Center on inflated-tube configurations indicated a possible design approach for the recovery of spacecraft and for aerial delivery of cargo. The need for research information on conical parawings for support of the Gemini parawing and the Army cargo-drop glider prompted extensive wind-tunnel research on inflated-tube type of wing configurations (see refs. 19, 28, and 24). Other work on wings having small leading edges and a rigid frame led to the construction of flight vehicles such as the paraglider Research Vehicle (ref. 17), the Ryan Flex-wing (refs. 13 and 20),

Army tow glider (ref. 26), and led to studies of parawing recovery of the Saturn booster (ref. 18). As indicated in figure 1, the highest lift-drag ratio that was obtained with conical parawings was about 7.0. Analysis of the test results and theoretical studies on conical parawings indicated that the relatively high drag of these wings was associated with the large variation of aerodynamic twist across the wing span. For some wings this washout at the tips was as high as  $60^\circ$ .

### Cylindrical Wings

A general research investigation was undertaken on a series of zero-twist cylindrical parawings having small, rigid leading edges (refs. 7 and 30). This investigation was undertaken to determine to what extent the lift-drag ratios could be improved by the use of a cylindrical canopy. The shaded area in the upper right-hand side of figure 1 shows that maximum lift-drag ratios as high as 17.0 were obtained with the small, tapered leading edge, cylindrical type of wing.

Interest in deployable wings that would provide lift-drag ratios greater than those obtained with the conical wings led to work on the advanced-concept cylindrical parawing which had tapered inflated-tube leading edges. These studies indicated that maximum lift-drag ratios from about 6 to 8 could be obtained with this type of wing.

### EFFECT OF ASPECT RATIO

The vertical spread in the shaded areas of figure 1 can be attributed to variations in aspect ratio and canopy fullness. Effects of aspect ratio on maximum lift-drag ratios for  $50^\circ$  swept parawings having conical and cylindrical canopies are summarized in figure 2.

### Conical Wings

Data for the conical wings on the left side of figure 2 show the critical nature of the leading-edge configuration on the maximum lift-drag ratios. Use of the very small, tapered leading edges allowed an increase in  $(L/D)_{\max}$  with increasing aspect ratio whereas the use of a slightly larger, untapered leading edge caused  $(L/D)_{\max}$  to decrease with increasing aspect ratio. A decrease in washout, which was obtained by reducing the canopy fullness, provided an increase in  $(L/D)_{\max}$  for the high-aspect-ratio wing having tapered leading edges. The test point shown for the inflated-tube, untapered leading-edge configuration (ref. 28) again indicates the level of  $L/D$  to be expected for this type of parawing.

## Cylindrical Wings

Considering now the cylindrical wings, shown on the right side of figure 2, it is evident that increasing the aspect ratio was much more effective in increasing  $(L/D)_{\max}$  than for the conical wings. A value of maximum lift-drag ratio of about 12 was obtained at high aspect ratio for the zero-twist wing with small tapered leading edges. By careful tailoring of the canopy to provide a small amount of washout, the maximum lift-drag ratio of this wing was increased to about 17.0. A comparison of the data for the conical and cylindrical wings having large leading edges (simulating inflated-tube designs) indicates that significant gains in  $(L/D)_{\max}$  can be realized for this type of wing by the use of a cylindrical canopy and tapered leading edges.

### FLARE TIME AND TOW VELOCITY FOR CONICAL AND CYLINDRICAL PARAWINGS

An important aerodynamic characteristic of conical and cylindrical parawings not shown in figure 2 is the minimum lift coefficient attainable before the onset of canopy luffing. This minimum  $C_L$  for conical wings has generally been found to be about 0.4, whereas for the cylindrical wings a minimum lift coefficient of around 0.2 is attainable. The next two figures present some information on how this lower value of  $C_L$  for the cylindrical wing can be used to an advantage.

#### Flare Time

The decision time available in a flared landing maneuver is presented in figure 3 as a function of preflare lift coefficient. Simplified approximate solutions are shown for three values of  $L/D$ . An approximate indication of the  $C_L$  and  $L/D$  combinations that are typical of conical and cylindrical parawings is shown by the shaded areas. A flight-data point obtained from reference 17 is shown by the symbol data point. Figure 3 was prepared to illustrate the fact that a significant increase in flare time should be possible by the use of a cylindrical wing having a low minimum lift coefficient, in comparison to a conical wing.

#### Tow Velocity

Flight velocity envelopes are shown for towed parawing vehicles as a function of wing loading in figure 4. The solid lines show the envelope for a  $50^\circ$  swept conical wing; the maximum speed is limited by the minimum  $C_L$  of 0.4 and the minimum landing speed is limited by  $C_{L_{\max}}$ . Data points are shown for the U.S. Army Towed Utility Glider (TUG).

The dashed curve of figure 4 shows the increase in tow speed available when the lower minimum  $C_L$  of the cylindrical wing is used. For example, at  $W/S = 6$  the tow speed can be increased from about 65 knots to about 95 knots by

use of a cylindrical wing. Although not shown in the figure, the higher  $L/D$  of the cylindrical wing would also allow a 30-percent reduction in tow force at the same wing loading.

#### STATIC WIND-TUNNEL DATA FOR LARGE LEADING-EDGE CYLINDRICAL PARAWING

Test results on conical and cylindrical parawings having small tapered leading edges are presented in references 7 and 30. However, data on cylindrical wings with large tapered leading edges have not been published. Figure 5 has therefore been prepared to present some typical wind-tunnel data on a  $50^\circ$  swept rigid-tube model which simulated this type of parawing. A structural design study for an inflated-tube cylindrical wing was made and the results of this study were used to obtain the size and shape of the wing leading edge.

#### Longitudinal Characteristics

The static longitudinal aerodynamic characteristics are presented on the left side of figure 5 ( $L/D$  is presented in fig. 2) for a low and a high aspect ratio. The lift curves show that a maximum lift coefficient of about 1.5 was obtained. Pitching moments for the aspect-ratio-2.5 wing show increasing stability at high lift, whereas the aspect-ratio-5.4 wing showed the well known instability of high-aspect-ratio sweptback wings at high lift. Results for both aspect ratios showed undesirably high negative values of pitching-moment intercept at zero lift,  $C_{m_0}$ . A large negative value of  $C_{m_0}$  could cause adverse stick-force gradients for some applications and could cause problems in maintaining separation of the wing and payload in the deployment of cable-suspended configurations.

#### Static Lateral Stability Characteristics

Static lateral stability derivatives given in the right-hand plot of figure 5 are presented with respect to a moment reference located on the keel center line at the mean aerodynamic quarter chord  $\bar{c}/4$ . Inasmuch as interpretation of these derivatives in terms of expected flight behavior is difficult, derivatives for an aspect-ratio-3 conical wing are also presented to illustrate these derivatives for a wing that has been found to have generally satisfactory flight behavior.

The directional stability derivative  $C_{n\beta}$  was somewhat lower for both cylindrical wings at low angles of attack than for the aspect-ratio-3 conical wing. Throughout most of the higher angle-of-attack range the static directional stability was somewhat higher for the cylindrical wings than for the conical wing. Large differences in the derivatives  $C_{y\beta}$  and  $C_{l\beta}$  were indicated at moderate and high angles of attack for the two types of wing canopy shape. Flight tests of cylindrical wings have not been made at the Langley Research Center; however, there are indications from other parawing configurations that the combination of lateral derivatives shown in figure 5 for the cylindrical

wings may give rise to dynamic lateral stability problems. These problems could be serious enough to require the use of auxiliary stabilizing surfaces.

## EFFECT OF CANOPY LOBE HEIGHT ON DEEP STALL CHARACTERISTICS OF A CONICAL WING

### Wing-Along Aerodynamic Characteristics

The variation of lift and pitching-moment coefficients with angle of attack are presented in the left-hand plot of figure 6 for a rigid-tube model having  $55^\circ$  sweep and large-diameter leading edges and keel. Data are presented for wing canopies having high lobes and low lobes. Test results for these wings in the normal operating angle-of-attack range are presented in reference 28.

The lift curves for the two canopy lobe heights show marked differences at angles of attack greater than about  $52^\circ$ . The results for the low-lobe canopy show an abrupt stall and a large loss of lift at about  $52^\circ$ ; whereas the high-lobe wing showed a gradual stall with very little loss of lift at the highest test angles of attack. The beneficial effect of the high-lobe canopy on the lift characteristics is believed to be associated with the favorable effect of the increased washout over the outboard part of the more highly twisted high-lobe wing.

The pitching moments for the wing alone are presented about a moment reference on the keel center line, at the  $\bar{c}/4$  of the projected  $55^\circ$  swept wing planform. Very little difference in wing-alone pitching moments was indicated for the two canopy lobe heights shown; however the low-lobe wing showed a stable break in the pitching moments at stall. These wing-alone data have been transferred to a low center-of-gravity position in order to indicate the characteristics of a cable suspended configuration, and the results are presented in the top part of the right-hand plot of figure 6. The assumed center-of-gravity positions were selected so that both wing configurations would be trimmed at  $C_L = 1.4$ .

### Stability and Trim of Complete Configuration

Pitching moments for the complete configuration with a high-lobe canopy showed a stable variation with angle of attack up to about  $67^\circ$ . Results for the low-lobe canopy, on the other hand, showed an instability below stall, a large pitch-up tendency at stall, and a stable trim point at about  $63^\circ$  angle of attack. The longitudinal stability and trim characteristics of the wing with the low-lobe canopy are considered to be highly undesirable because the deep-stall trim point could be reached inadvertently as a result of the instability that occurred before stall and at stall.

Reasons for this instability with the low-lobe canopy are not apparent in the wing-alone characteristics; however, an examination of the axial-force characteristics can provide an explanation. For the high-lobe canopy, the axial force was negative and became more negative as the angle of attack increased. The low-lobe wing, on the other hand, showed a large loss in axial force (loss of force in the forward direction) at wing stall; this large reduction in axial force, multiplied by the large vertical moment-arm, caused the pitch-up tendency encountered on the low-lobe wing.

The low-lobe wing of figure 6 was selected as a configuration of interest because it provided the highest value of  $(L/D)_{\max}$  from a range of conical canopy shapes investigated in the tests of reference 28. The deep stall characteristics of this low-lobe wing were, however, so undesirable that the use of this canopy may not be feasible for some types of parawing vehicles. These results indicate that other factors besides the maximum lift-drag ratio must be evaluated in the selection of a wing canopy and that serious deficiencies in stability, trim, or control characteristics may require consideration of canopy shapes that provide somewhat less than the best possible lift-drag ratios.

#### EFFECTS OF WING SWEEP ON $(L/D)_{\max}$ AND SPREADER-BAR LOADS

The preceding discussion considered a possible wing design for which the stability and trim problems associated with the canopy shape for best performance made it undesirable to select the best-performance configuration. If the penalties associated with the best-performance configuration are appreciable and the attainment of maximum performance is not a primary goal, then alternate wing configurations should be explored in an attempt to obtain a rational wing design that will have acceptable performance and satisfactory stability characteristics and structural loads requirements. Figure 7 has been prepared to illustrate some possible design trade-offs involving structural loads, performance, and wing sweep. The variations of  $(L/D)_{\max}$  with wing sweep and the variation of spreader-bar load coefficient with  $C_L$  for three selected wings were obtained from reference 28. The coefficients presented are based on the projected plan-form area of the  $55^\circ$  swept wing.

The variation of  $(L/D)_{\max}$  with sweep angle is presented for three families of wings having different canopy flat pattern sweep angles. It is apparent that there are different combinations of wing sweep and flat-pattern sweep that will provide the same value of  $(L/D)_{\max}$ . Three such possible wings have been identified by the symbols which indicate wing configurations that will provide an  $(L/D)_{\max}$  of approximately 4.0. Since these wings provide about the same performance, other design requirements can be evaluated to determine the most desirable combination of design parameters.

One important factor in the design of a parawing which has its sweep angle fixed by a spreader bar is the axial load in the spreader bar. Spreader-bar load coefficients are presented in figure 7 for the three wings identified by the symbols in the left-hand plot. The axial load in the spreader bar was

compressive throughout the test lift-coefficient range for the 50° swept wing (indicated by the circle symbols) and was fairly high at low-lift coefficients. Increasing the sweep to 55° greatly reduced the axial load at low lift, and at high lift the spreader-bar load changed from compression to tension (square symbols). For the 60° swept wing (diamond symbols) fairly high values of spreader-bar tension were indicated at high lift, which suggests the possibility that a spreader bar may not be required for such a configuration. Of course for a cable-supported payload, the side component of cable tension would add a positive increment to the aerodynamic input from the canopy (CSB) and would be balanced either by compression in the spreader bar or by the tension (opening force) from the canopy.

The spreader-bar load data of figure 7 indicate that for the three wings shown (each provides  $(L/D)_{\max}$  about 4), the structural design problems should be less severe for the more highly swept wings. With regard to the use of parawings without a spreader bar, these data also suggest that equilibrium sweep angles (at CSB = 0) will exist for cable supported payloads such that low sweep angles will be in equilibrium (cable side load balanced by aerodynamic opening force of the canopy) at high lift, and high sweep angles will be in equilibrium at low lift. This principle of equilibrium sweep angle was used in early tests at the Langley Research Center on parawings having keel lengths up to 50 feet and for payload weights up to 3000 pounds. (See ref. 3.) A more recent application of this principle has been in the precision-drop glider under development by the U.S. Army for aerial delivery of cargo. (See ref. 31.)

#### U.S. ARMY PRECISION DROP GLIDER

A sketch of the Army drop glider is given in figure 8 to show the general arrangement of the configuration which was designed and constructed by the Ryan Aeronautical Co. This cargo delivery system was designed for a payload of 300 pounds which is contained in a rectangular box attached to the bottom of the wing control platform. Four riser straps are shown attached to the sides of the control platform and the suspension lines from the wing are attached to the risers.

The wing has 6-inch-diameter inflated-tube leading edges and keel, which are 22 feet long, and a cloth lifting surface. Air for inflating the leading edges and keel is supplied by a high-pressure storage bottle in the rear of the keel. Directional control is achieved by pulling on the suspension line on either wing tip and is actuated by a motor in the control platform. The control system was designed for steering by radio command from a ground or air controller, or by an automatic homing system that seeks a radio beacon located on the ground in the target drop area.

The wing is folded in a compact package similar to a parachute pack and is located in the control platform before deployment. The cargo box and packaged wing are discharged from an aircraft, and wing deployment is initiated by a static line. Deployment loads are attenuated by use of an initial parachute-like phase. After the tubes have been inflated the reefing lines are cut, and

the wing completes deployment into the configuration shown in figure 8 and then makes a transition from vertical flight to gliding flight.

This program has been successful in demonstrating the feasibility of aerial delivery of cargo by means of a deployable parawing. It is anticipated that development of this use for a parawing will continue and additional controls can be included to provide flare capability for reduction of landing speeds.

## LIMP PARAGLIDERS

The Army drop glider represents a minimum-structure configuration in the overall spectrum of paragliders presented in figure 1. The success of this type of wing and recent emphasis on gliding parachutes for personnel and recovery of manned spacecraft has prompted a renewed research effort on the original paraglider concept for a completely flexible lifting surface. Parawings having no rigid structural parts may be referred to as limp paragliders or wing-type gliding parachutes, and may be considered to include present gliding parachutes of various names in view of the definition of a parawing, which is: A flexible lifting surface that has the structural characteristics of a parachute and the aerodynamic characteristics of a wing.

Recent research on limp paragliders has been conducted at the Langley Research Center on configurations similar to that shown in figure 9. This work has included both static wind-tunnel tests and free-glide helicopter drop tests. Work on deployment mechanics and deployment loads has been done in both wind-tunnel and drop tests. As of July 1, 1965, 86 successful free-drop deployments out of 86 tries from a fully packaged condition have been made. Most of the wind-tunnel tests have been made on wings having a 5-foot keel length; deployments and glide tests have been made on models having keel lengths of 5, 8, 12, and 24 feet.

Photographs of some of the flight-test operations for free-drop tests of the 24-foot limp paraglider are shown in the photographs of figures 10 to 12. The method of checking for line entanglement after retrieval and before repacking is illustrated in figure 10 and the method of folding the wing for packing is shown in figure 11. A photograph of the 24-foot wing in the deployment bag suspended from the cargo hook of a helicopter, and the payload of 300 pounds of lead suspended from the deployment bag is shown in figure 12. Successful deployment drops of the 24-foot wing from a helicopter have been made with payload weights of 100, 200, and 300 pounds, which gave a wing-loading range from 0.25 to 0.75. The wing which was made of nonporous, 1.1-ounce coated parachute nylon had 400 square feet of area and weighed approximately 5 pounds with all line attachments, but not including the standard personnel parachute nylon lines.

### Wind-Tunnel Tests of 5-Foot Limp Paragliders

Static wind-tunnel tests of a variety of wing planforms have been made and some of the planform variations studied are shown in figure 13. Flat-pattern sweep angles of  $40^\circ$ ,  $45^\circ$ , and  $50^\circ$  were investigated on wings having leading edges

and keel of equal length. Early flight tests indicated a tendency for the nose to collapse when the planform extended to the apex and therefore the apex was cut off as shown in the sketches of figure 13. Variations in the  $45^\circ$  swept planform included addition of a  $1.25l_k$  radius to the leading edges and a  $1.0l_k$  radius to the trailing edge. A  $45^\circ$  swept slotted wing was formed by overlapping panels of fabric which were joined only at the leading edges and keel. Test results were also obtained on a  $45^\circ$  swept wing having a flat pattern aspect ratio of 5.2 and a  $45^\circ$  delta planform. A fabric tube, closed at the front end was attached to the top of the keel of the  $45^\circ$  delta wing. Ram-air inflated the tube through an inlet located near the rear of the keel on the bottom surface. Flat-braided nylon rope was attached to the upper surface of another wing, with a parabolic shape between line-attachment points as shown in figure 13. Tests of this wing were made with the basic straight leading edge and with the fabric removed to the parabolic line.

Effect of flat pattern sweep.- Wind-tunnel data obtained with the three flat-pattern sweep angles investigated are presented in figure 14. These results show that both the  $40^\circ$  and  $45^\circ$  swept wings provided lift-drag ratios of about 2.4, whereas the  $50^\circ$  swept wing gave a value of about 2.1. None of the completely flexible wings appeared to have substantially better characteristics than the original  $45^\circ$  swept wing with the front  $l_k/8$  removed, and this wing was therefore selected as a basic configuration for more detailed study.

Effects of dynamic pressure and line stretch.- The lift coefficients presented in figure 14 showed an appreciable variation with test dynamic pressure. Part of this variation was probably due to stretch in the nylon lines and in the canopy. The test results presented in figure 15 show a comparison of data obtained with steel cables and with nylon lines. At dynamic pressures above  $q = 1.0$  there was very little variation with dynamic pressure of lift coefficient or angle of attack for the model with the steel cables. At dynamic pressures below about 1.0 there was a variation in lift coefficient that may have occurred because the dynamic pressure was not high enough to minimize effects of the weight of the steel cables and the wing canopy. (See ref. 19.) In general, the lift coefficient and angle of attack were slightly lower with the steel cables and the lift-drag ratios obtained with the steel cables were slightly higher than with the nylon lines. A higher lift-drag ratio would be expected with the steel cables inasmuch as the diameter of the cables was one-half the diameter of the nylon lines and the total frontal area of the nylon lines was about 100 square inches.

Experimental and estimated drag.- A comparison of experimental and estimated drag coefficients and lift-drag ratios are given in figure 16. Estimates of skin friction and line-drag increments were assumed to be invariant with lift coefficient as shown. The drag due to lift was assumed to be that given by full leading-edge suction,  $\Delta C_D = C_L^2 / \pi A$ , where the aspect ratio was obtained by use of the actual model span measured during the tests and the flat-pattern area. Estimated lift-drag ratios were obtained from the estimated total drag coefficients and are shown in the top portion of figure 16.

The level of the experimental lift-drag ratios at a given lift coefficient appear reasonable when compared to the estimated curve, which may be considered

as an upper boundary for the aspect ratio and minimum drag used. The maximum lift-drag ratios obtained in the experimental results as indicated by the faired data were much lower than the estimated value of  $(L/D)_{\max}$ . The reason that the experimental values of  $(L/D)_{\max}$  were low lies in the fact that the wing could fly with a stable canopy shape at lift coefficients near 1.0, and attempts to fly the wing at lift coefficients much less than 1.0 caused the nose of the wing to collapse. The amount of nose collapse appeared to increase as the lift coefficient decreased after initial collapse occurred, and the drag and angle of attack increased as nose collapse became more extensive.

The three test points in figure 16 labeled "keel batten" were obtained with the keel reinforced by a 10-mil mylar batten to prevent early collapse of the nose of the wing. These test results show that maximum lift-drag ratios of around 3.0 on a limp paraglider were obtained by the addition of some local stiffening at the keel.

Modulation of Lift and Lift-Drag Ratio.- Some of the results discussed in the previous figure were obtained with the nose collapsed and it is of interest to determine to what extent the lift coefficient can be varied without the occurrence of nose collapse. Results are presented in figure 17 to indicate the extent that  $C_L$ , angle of attack, and  $L/D$  have been varied in wind-tunnel tests for a completely flexible limp paraglider. For these tests, only the lengths of the wing-tip and keel trailing-edge lines were varied as indicated in the top part of figure 17. The initial angle of attack and rigging condition selected was the condition for the maximum  $L/D$  just before the nose started to tuck under. The line lengths were shortened from this condition to provide progressive increases in angle of attack. The trim angle-of-attack range was from about  $26^\circ$  to  $41^\circ$ , for which the lift-drag ratios varied from 2.4 to 1.2. The maximum angle of attack was limited in the tunnel tests to angles for which the model was trimmed and had longitudinal and lateral stability. Experience with static wind-tunnel and free-glide tests of the same wing has indicated that the infinite-mass payload constraint in the tunnel tests may impose somewhat more severe stability problems than the free-flight condition where the payload can respond to disturbances. It is therefore believed that the range of angle of attack for trimmed flight may be somewhat higher than that indicated in the wind-tunnel tests.

Line-tension coefficients.- The critical design line loads for a deployable wing will, of course, be expected to occur during deployment; however, the distribution of line tension for steady-state glide conditions is also important from the standpoint of canopy loading and rigging geometry. Some typical line-tension-coefficient data are presented in figure 18 as a function of the distance of the line attachment from the theoretical wing apex.

The highest loadings for both the keel lines and the leading-edge lines appear to occur at the 60-percent location and most rearward lines. Increasing the angle of attack was found to cause the wing-tip lines and keel trailing-edge line to carry a somewhat higher load in relation to the other lines than shown in figure 18. The use of fairly elastic lines such as nylon parachute lines gives rise to rigging problems not encountered on a conventional parachute because the line tension varies appreciably from line to line. This unequal

tension distribution causes unequal stretch in the elastic lines and has to be properly accounted for in obtaining the proper rigging. Early flight experience with increasing payload weight indicated that shortening of the three rear lines to account for line stretch had to accompany increases in payload weight in order to obtain a similar canopy shape in flight. This same effect has been observed in wind-tunnel tests as the dynamic pressure was increased when nylon lines were used, whereas these rigging corrections did not have to be made when the steel cables were used.

The three rear lines have been found to be the most important lines with regard to rigging for a stable canopy shape and trimmed flight. As noted in the discussion of figure 17, longitudinal control can be achieved by changing the lengths of the three rear lines. It is anticipated therefore, that these lines would be controllable and that both trim and lift modulation would be accomplished by changing the lengths of these lines.

Roll control.- Free-flight tests of limp paragliders have indicated that directional control could be easily obtained by shortening the length of the wing-tip line to the wing on the inside of the desired turn (e.g. shorten the right tip line to produce a right turn). These flight tests, conducted on configurations having a point suspension, indicated that a wing rigged for straight flight could be trimmed to provide a gentle turn or a tight spiral by progressive shortening of one tip line. Inasmuch as quantitative data on turn performance were not obtained in these flight tests, it was considered desirable to obtain information on lateral-directional control effectiveness in the wind-tunnel studies. The wind-tunnel data from these tests are presented in figure 19 in terms of wing bank angle as a function of line shortening from the 0° bank initial trim position. The sketch in figure 19 shows a rear view of the model on the support strut and the modified attachment for the wing-tip lines. The wing-tip lines were spread in order to allow trimmed steady-state bank angles to be obtained. With a point suspension (no lateral spread of the tip-line attachments), no restoring moments could be generated to oppose the wing rolling moment and the wing would tend to autorotate.

The test results presented in figure 19 show that the control effectiveness was linear for bank angles up to about 40° and that the effectiveness was the same with differential control as with shortening of only one line. The observation was made during these tests that the directional stability of the wing allowed very little sideslip even for the highest roll angles reached.

#### Deployment Loads on 5-Foot Limp Paragliders

Some preliminary deployment-loads tests have been made with a 5-foot limp paraglider model using a "Cherry Picker" to obtain the drop height of between 80 and 90 feet. Measurement of total deployment load was obtained by means of a tension gage which connected the payload to the line confluence point. Data were obtained with a ground-based recording oscillograph which recorded the output of the tension gage by means of a lightweight trailing electrical cable. A sample deployment-load time history is presented in figure 20 for a drop in which a free fall of about 30 feet before initiation of deployment was obtained

by use of a 30-foot static line attached to the deployment bag. The time history shows that line extraction occurred about 1.5 seconds after release and the lines were fully extended 0.2 second later when the wing began to extract from the deployment bag. Wing filling began about 0.1 second after wing extraction began and the peak deployment load occurred about 0.2 second after the beginning of wing filling. Transition from vertical flight to gliding flight began during the wing deployment phase ( $t = 1.9$  to  $t = 2.0$ ). At  $t = 2.2$  the wing was seeking its equilibrium glide speed and the force-to-weight ratio oscillated about a value of 1.0 until trimmed glide speed was attained.

The relatively fast deployment of the wing (approximately 0.5 second from beginning of line extraction to end of deployment load) indicates that the limp paraglider may be useful where rapid deployment is desired. The rapid deployment however implies high deployment loads when a large amount of energy is to be absorbed. Conditions of relatively high deployment velocities have not been studied because of the drop-height limitation of the Cherry Picker used in the tests. The peak load shown in figure 20 of about 7 times the weight appears high when consideration is given to the fact that the dynamic pressure at the start of wing filling was only about 3 pounds per square foot, and a realistic value for some applications may be 30 times as large as the dynamic pressure of these tests. It is therefore believed that methods of attenuating the deployment load will have to be devised in order to deploy the limp paraglider at high dynamic pressures.

Some limited deployment tests have been made in the wind tunnel to study the effects of dynamic pressure for an infinite-mass payload condition, and typical results from these tests are presented in figure 21. The left-hand plot shows the variation of total load with time from wing filling for several test dynamic pressures. The maximum dynamic pressure was limited by the nominal 100-pound limit of the tension gage used to measure the load. The test results indicated that the load profiles appeared similar and increased proportionally with increasing dynamic pressure. The time for attainment of peak load appeared however to decrease slightly as the dynamic pressure increased.

Three deployments were made at each dynamic pressure and the average of the peak loads obtained are plotted in the right-hand plot of figure 21. The variation of average peak load with dynamic pressure suggested a constant coefficient  $C_F$  as also plotted in figure 21. The deployment force coefficient had a value of about 3.8, and represents a transient force coefficient rather than a steady-state value. As in the free-flight deployments, the wing began a transition to gliding flight during deployment and since the deployment was parallel to the longitudinal axis of the tunnel, steady-state conditions were not achieved after deployment. Interpretation of these deployment loads obtained in the wind tunnel is difficult because of the infinite-mass payload condition of the tests. It is hoped that further wind-tunnel and free-drop deployments can be used to provide an indication of correlating factors for the total load, so that measurements of individual line loads can be made in wind-tunnel deployments to identify critical lines from the standpoint of deployment load.

## Limp Paraglider State of the Art and Problem Areas Requiring Research

Typical data have been presented on the aerodynamic characteristics of limp paragliders as obtained in the 17-foot test section of the Langley 300 mph 7- by 10-foot tunnel. The wind-tunnel and flight tests have demonstrated that a canopy made of flexible parachute nylon and having a sweptback-wing type of planform can be rigged with suspension lines to provide stable gliding flight and can be deployed from a packaged condition in a manner similar to a conventional parachute. Lift-drag ratios of 2.5 were obtained on a completely flexible wing and could be increased to 3.0 or 3.5 by the use of a semiflexible batten in the keel, or by use of a ram-inflated fabric tube on the keel.

Inasmuch as the limp paraglider has received only recent research emphasis, there are several important problem areas that have not received attention, or require expanded research effort. The problem areas requiring research emphasis are as follows:

- A. Deployment                      Reduction of total load by reefing or sequencing of deployment. Determination of line loads for realistic dynamic pressures.
- B. Control                            Increase range of  $C_L$  and L/D modulation. Proper simulation of line attachments for spacecraft and cargo. Determine control forces, vehicle response rates.
- C. Stability                          Define longitudinal and lateral stability characteristics over  $C_L$  range. Investigate stability in near vertical descent.
- D. Performance                      Determine requirements for L/D and wing loading for satisfactory glide landing and flared landing.
- E. Aeroelasticity                    Determine scale effects and W/S effects on rigging. Determine model simulation laws for deployment, glide and landing.
- F. Fabrication                        Transfer of load from line attachment into canopy. Seam and fabric reinforcement techniques.

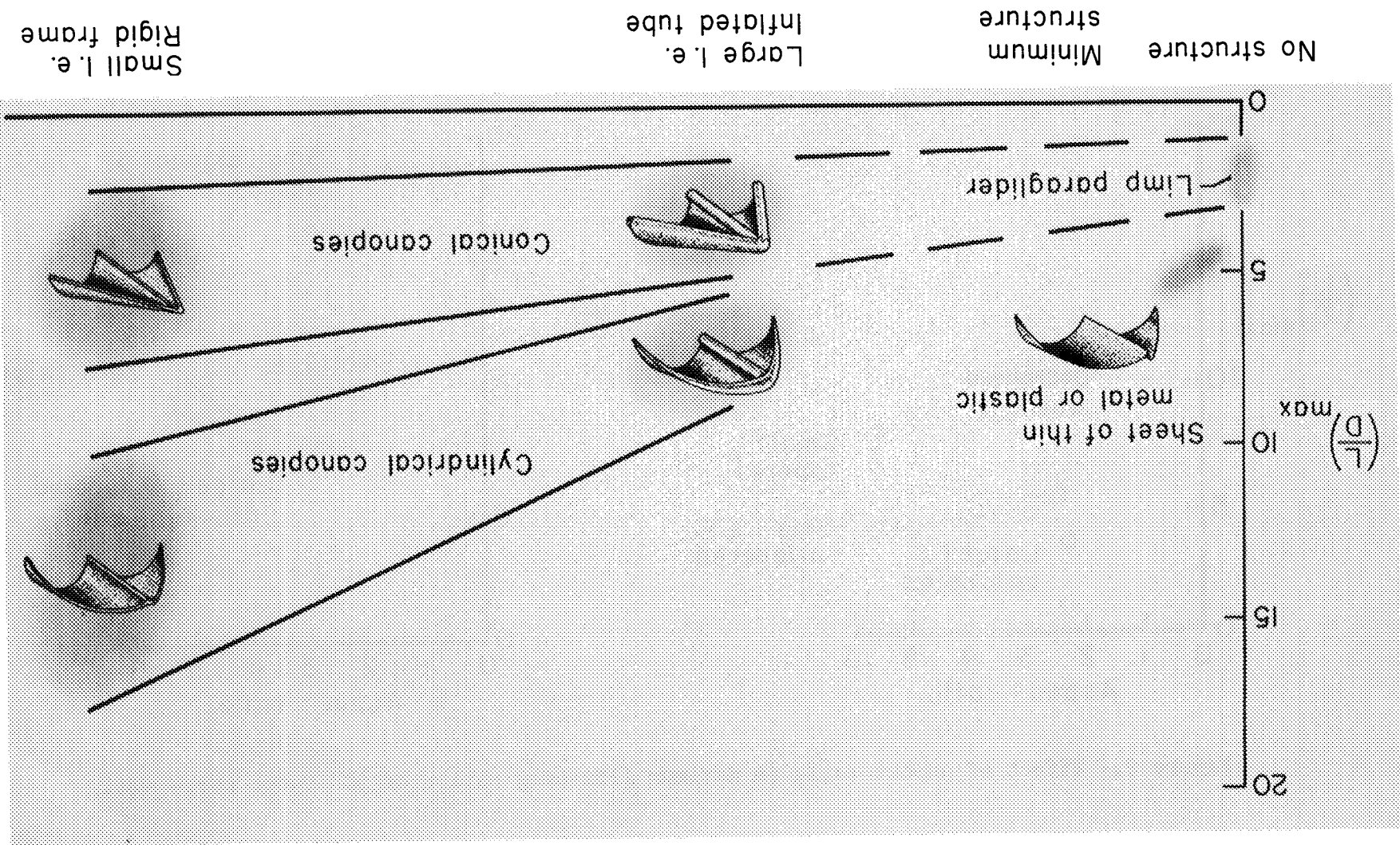
LIST OF REFERENCES AND BIBLIOGRAPHY OF PARAGLIDER PUBLICATIONS

1. Rogallo, Francis M.: Introduction to Aeroflexibility. Presented April 21, 1954 to ARDC Reserve Unit at Langley Field, Va.
2. Rogallo, Francis M.: Paraglider Recovery Systems. Presented at IAS Meeting on Man's Progress in the Conquest of Space. St. Louis, Missouri, April 30, May 1-2, 1962.
3. Rogallo, Francis M.: Flexible Wing Research and Development. Presented at the Symposium on Retardation and Recovery. Dayton, Ohio, November 13-14, 1962.
4. Rogallo, Francis M., Lowry, John G., Croom, Delwin R., and Taylor, Robert T.: Preliminary Investigation of a Paraglider. NASA TN D-443, 1960.
5. Naeseth, Rodger L.: An Exploratory Study of a Parawing as a High-Lift Device for Aircraft. NASA TN D-629, 1960.
6. Hewes, Donald E.: Free-Flight Investigation of Radio-Controlled Models With Parawings. NASA TN D-927, 1961.
7. Polhamus, Edward C., and Naeseth, Rodger L.: Experimental and Theoretical Studies of the Effects of Camber and Twist on the Aerodynamic Characteristics of Parawings Having Nominal Aspect Ratios of 3 and 6. NASA TN D-972, 1963.
8. Fournier, Paul G., and Bell, B. Ann: Low Subsonic Pressure Distributions on Three Rigid Wings Simulating Paragliders With Varied Canopy Curvature and Leading-Edge Sweep. NASA TN D-983, 1961.
9. Taylor, Robert T.: Wind-Tunnel Investigation of Paraglider Models at Supersonic Speeds. NASA TN D-985, 1961.
10. Hatch, Howard G., Jr., and McGowan, William A.: An Analytical Investigation of the Loads, Temperatures, and Ranges Obtained During the Recovery of Rocket Boosters by Means of a Parawing. NASA TN D-1003, 1962.
11. Fournier, Paul G., and Bell, B. Ann: Transonic Pressure Distributions on Three Rigid Wings Simulating Paragliders With Varied Canopy Curvature and Leading-Edge Sweep. NASA TN D-1009, 1962.
12. Penland, Jim A.: A Study of the Aerodynamic Characteristics of a Fixed Geometry Paraglider Configuration and Three Canopies With Simulated Variable Canopy Inflation at a Mach Number of 6.6. NASA TN D-1022, 1962.
13. Johnson, Joseph L., Jr.: Low-Speed Wind-Tunnel Investigation to Determine the Flight Characteristics of a Model of a Parawing Utility Vehicle. NASA TN D-1255, 1962.

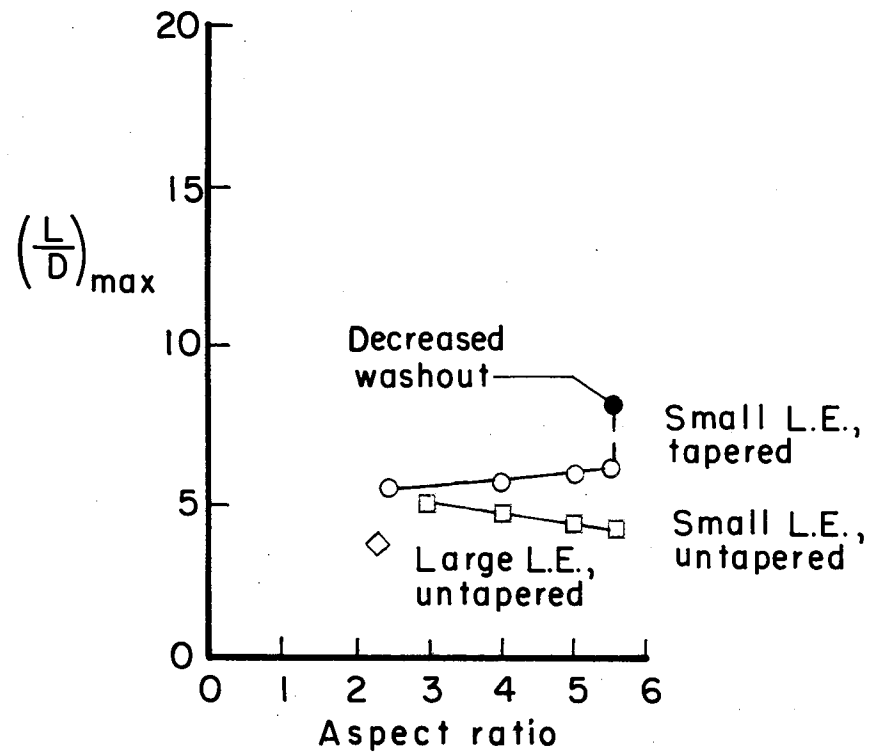
14. Shanks, Robert E.: Experimental Investigation of the Dynamic Stability of a Towed Parawing Glider Model. NASA TN D-1614, 1963.
15. Fournier, Paul G.: Pressure Distributions on Three Rigid Wings Simulating Parawings With a Varied Canopy Curvature and Leading-Edge Sweep at Mach Numbers From 2.29 to 4.65. NASA TN D-1618, 1963.
16. Wornom, Dewey E.; and Taylor, Robert T.: Aerodynamic Characteristics of a Flexible-Canopy Paraglider Model at a Mach Number of 4.5 for Angles of Attack to  $360^{\circ}$  and Sideslip Angles From  $0^{\circ}$  to  $90^{\circ}$ . NASA TN D-1776, 1963.
17. Layton, Garrison P.; and Thompson, Milton O.: Preliminary Flight Evaluation of Two Unpowered Manned Paragliders. NASA TN D-1826, 1963.
18. Burk, Sanger M., Jr.: Free-Flight Investigation of the Deployment, Dynamic Stability, and Control Characteristics of a 1/12-Scale Dynamic Radio-Controlled Model of a Large Booster and Parawing. NASA TN D-1932, 1963.
19. Sleeman, William C., Jr.: Low-Speed Investigation of Cable Tension and Aerodynamic Characteristics of a Parawing and Spacecraft Combination. NASA TN D-1937, 1963.
20. Johnson, Joseph L., Jr.; and Hassell, James L., Jr.: Full-Scale Wind-Tunnel Investigation of a Flexible-Wing Manned Test Vehicle. NASA TN D-1946, 1963.
21. Naeseth, Rodger L., and Gainer, Thomas G.: Low-Speed Investigation of the Effects of Wing Sweep on the Aerodynamic Characteristics of Parawings Having Equal-Length Leading Edges and Keel. NASA TN D-1957, 1963.
22. Sleeman, William C., Jr.; and Johnson, Joseph L., Jr.: Parawing Aerodynamics. Astronautics and Aerospace Engineering, June 1963.
23. Johnson, Joseph L., Jr.: Low-Subsonic Flight Characteristics of a Model of a Supersonic-Airplane Configuration With a Parawing as a Landing Aid. NASA TN D-2031, 1963.
24. Libbey, Charles E.: Free-Flight Investigation of the Deployment of a Parawing Recovery Device for a Radio-Controlled 1/5-Scale Dynamic Model Spacecraft. NASA TN D-2044, 1963.
25. Libbey, Charles E.; and Johnson, Joseph L., Jr.: Stalling and Tumbling of a Radio-Controlled Parawing Airplane Model. NASA TN D-2291, 1964.
26. Shanks, Robert E.: Experimental Investigation of the Dynamic Stability of a Towed Parawing Glider Air Cargo Delivery System. NASA TN D-2292, 1964.
27. Phillips, W. Pelham: Low-Speed Longitudinal Aerodynamic Investigation of Parawings as Auxiliary Lifting Devices for a Supersonic Airplane Configuration. NASA TN D-2346, 1964.

28. Croom, Delwin R., Naeseth, Rodger L.; and Sleeman, William C., Jr.:  
Effects of Canopy Shape on Low-Speed Aerodynamic Characteristics of a  
55° Swept Parawing With Large-Diameter Leading Edges. NASA TN D-2551.
29. Libbey, Charles E.: The Deployment of Parawings for Use as Recovery System  
Systems. Presented at the AIAA Aerospace Science Meeting. Washington,  
D.C., June 29-July 2, 1964.
30. Bugg, Frank M.: Effects of Aspect Ratio and Canopy Shape on Low-Speed  
Aerodynamic Characteristics of 50.0° Swept Parawings. NASA TN D-2922,  
1965.
31. Ryan Aeronautical Company: Flexible-Wing Precisian Drop Glider. U.S. Army  
Transportation Research Command Technical Report 63-64, 1963.
32. Rogallo, Francis M.: Parawings for Astronautics. Presented at the  
Specialist Meeting on Space Rendezvous, Rescue and Recovery.  
Edwards Air Force Base, California, September 10-12, 1963.

Figure 1.- Spectrum of parawings investigated and maximum lift-drag ratios obtained in wind-tunnel tests.



### CONICAL WINGS



### CYLINDRICAL WINGS

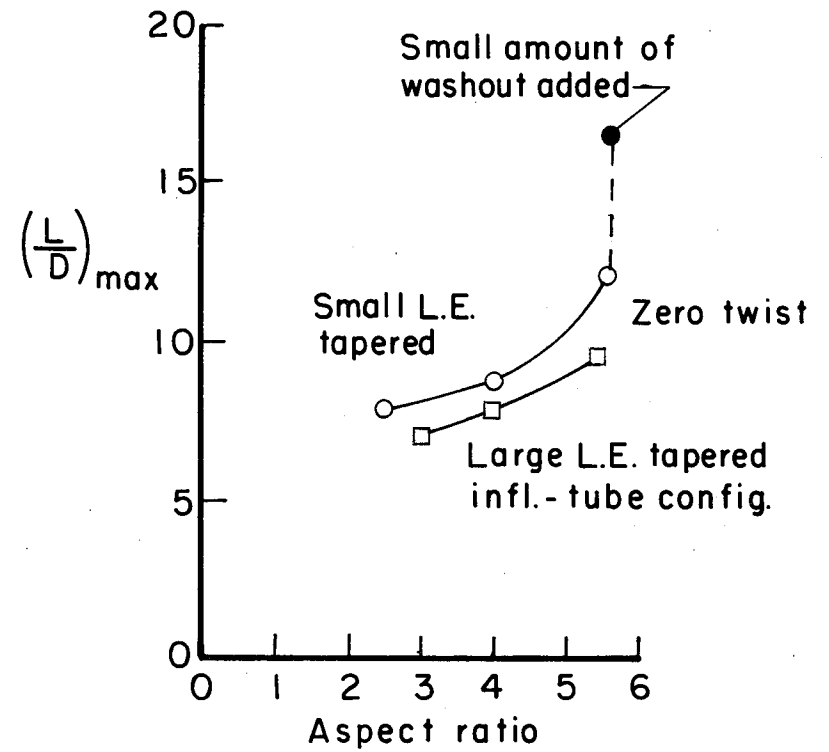


Figure 2.- Effect of aspect ratio on maximum lift-drag ratios of  $50^\circ$  swept parawings.

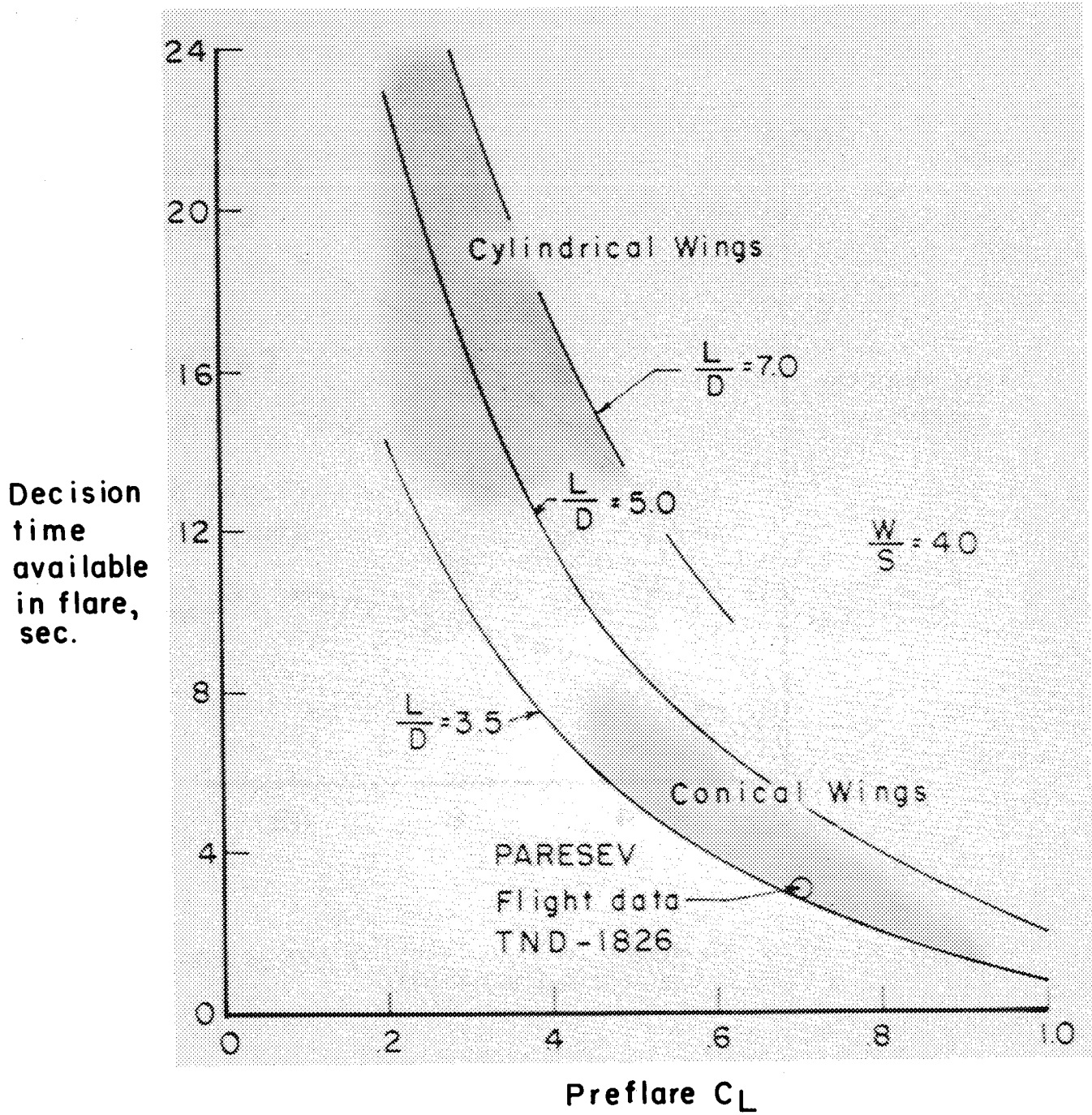


Figure 3.- Effect of minimum preflare lift coefficient on decision time available during flare.

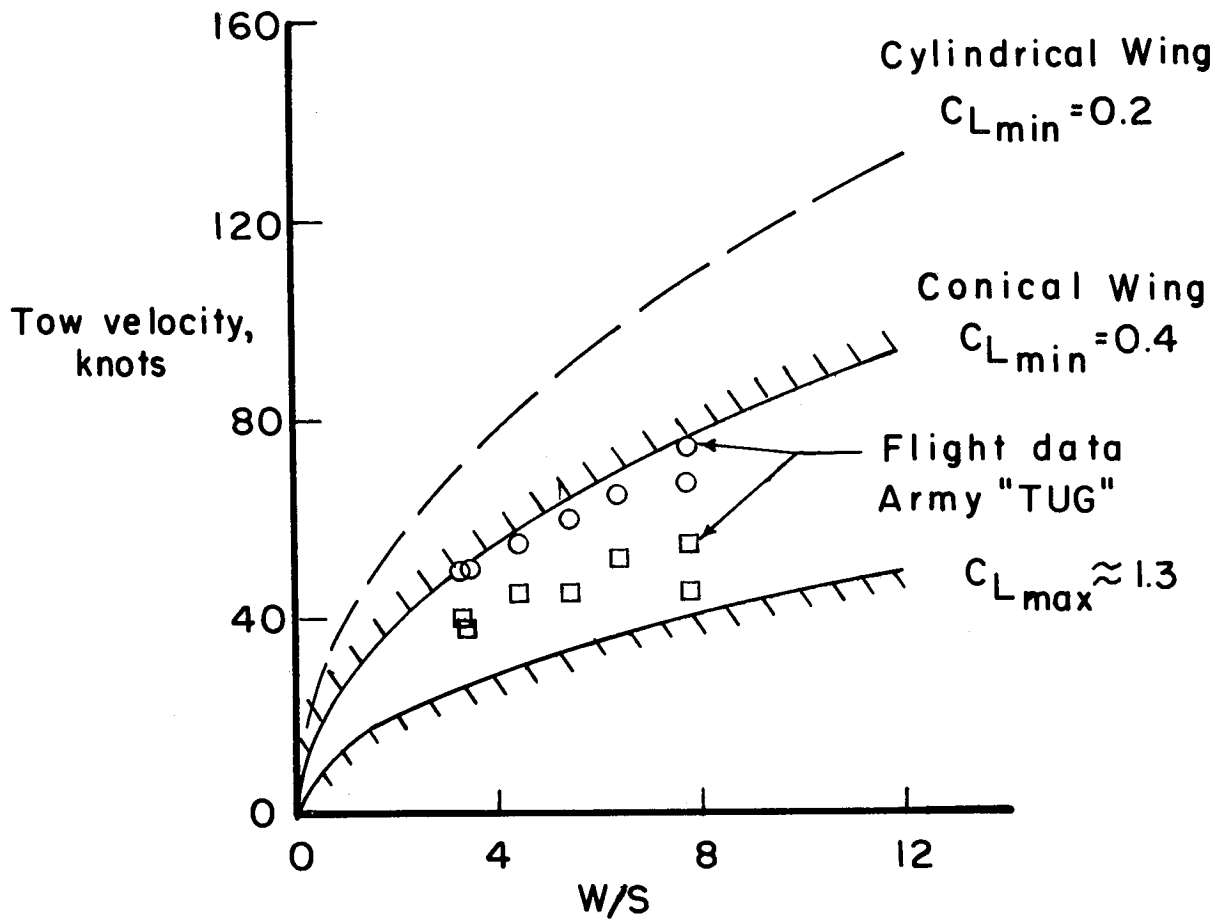


Figure 4.- Flight envelopes for towed vehicles having conical and cylindrical parawings.

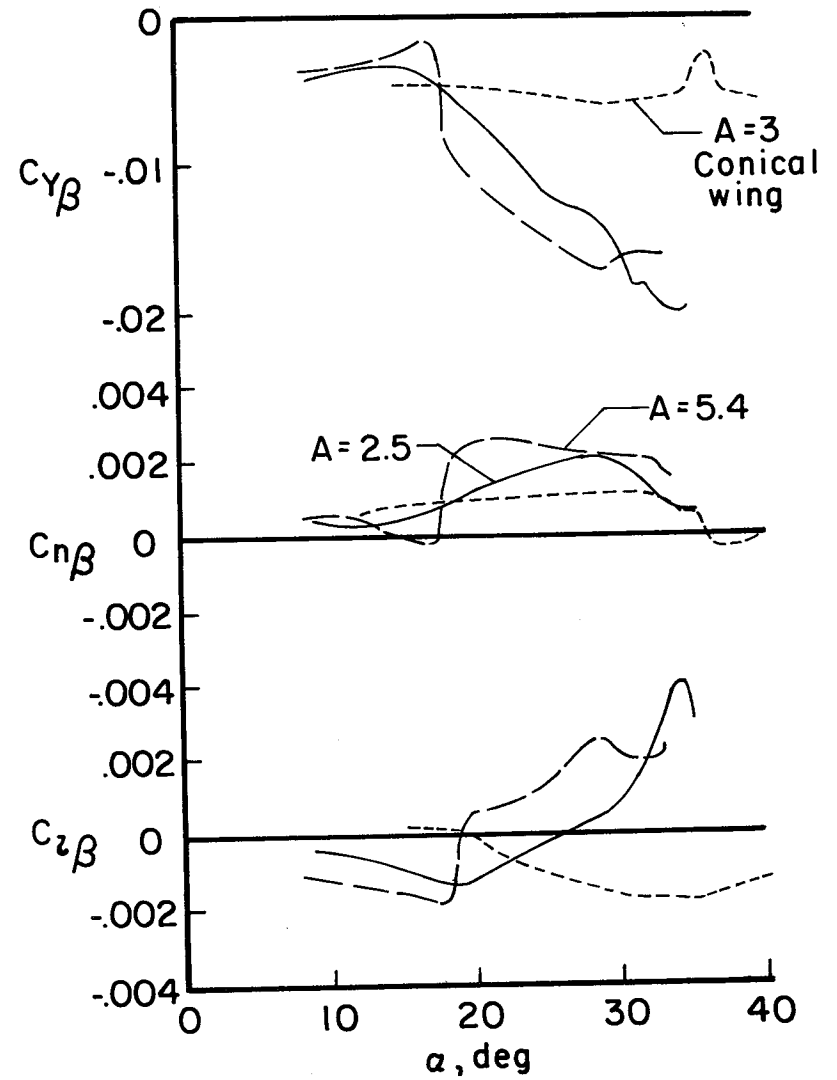
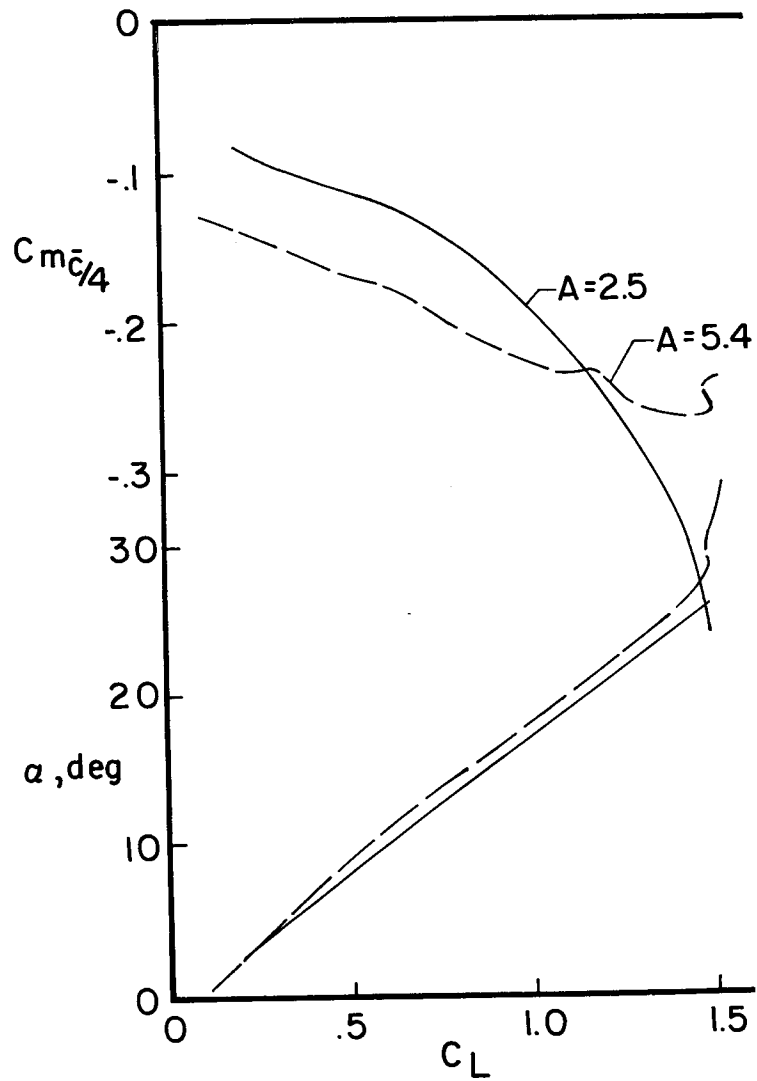


Figure 5.- Effect of aspect ratio on the static stability characteristics of a rigid-frame model simulating an inflated-tube cylindrical parawing.

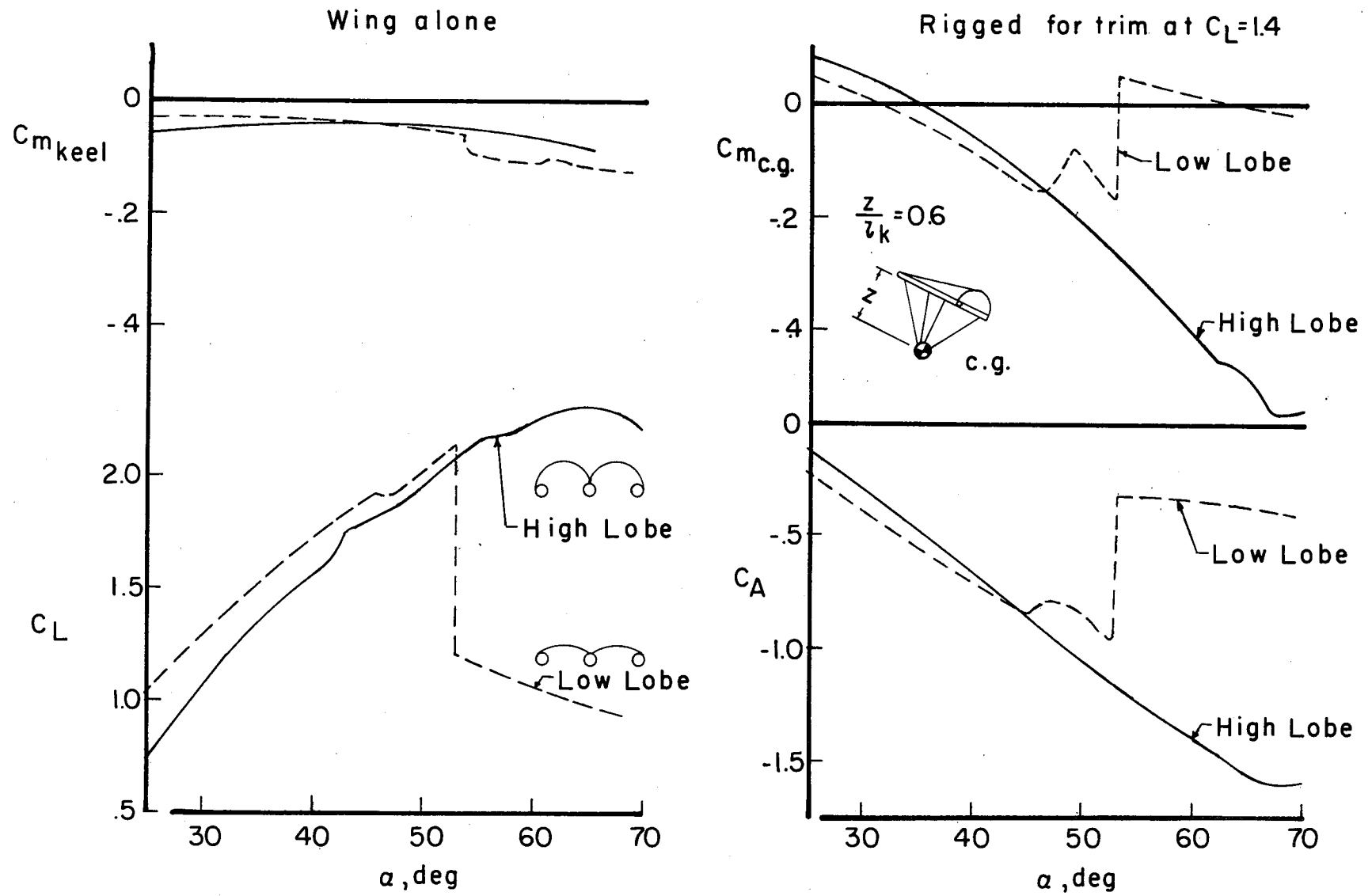


Figure 6.- Effect of canopy lobe height on the high angle-of-attack (deep-stall) stability and trim of a  $55^\circ$  swept conical parawing having large-diameter leading edges.

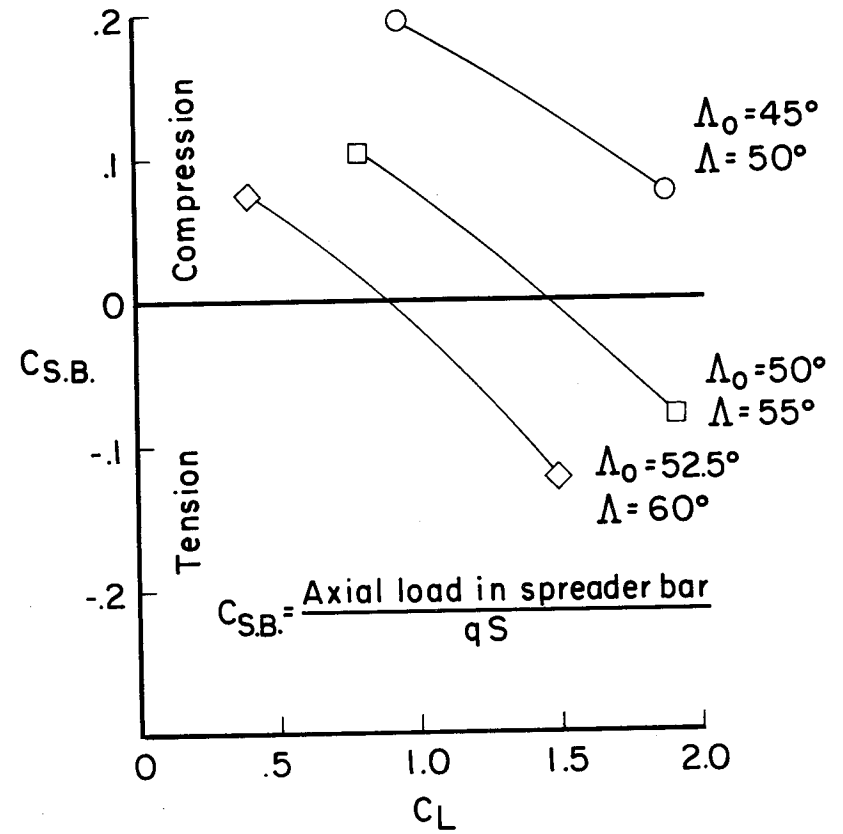
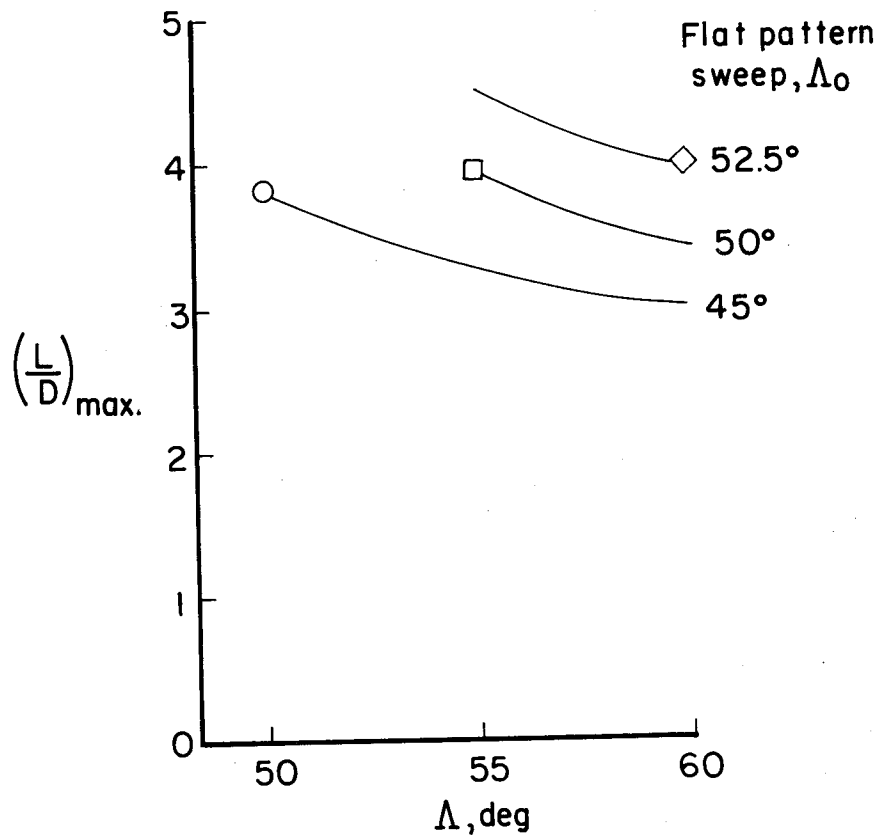
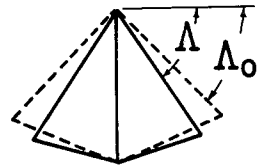


Figure 7.- Variation with sweep of maximum lift-drag ratios and spreader-bar axial load for large-diameter inflated tube conical parawing configurations.

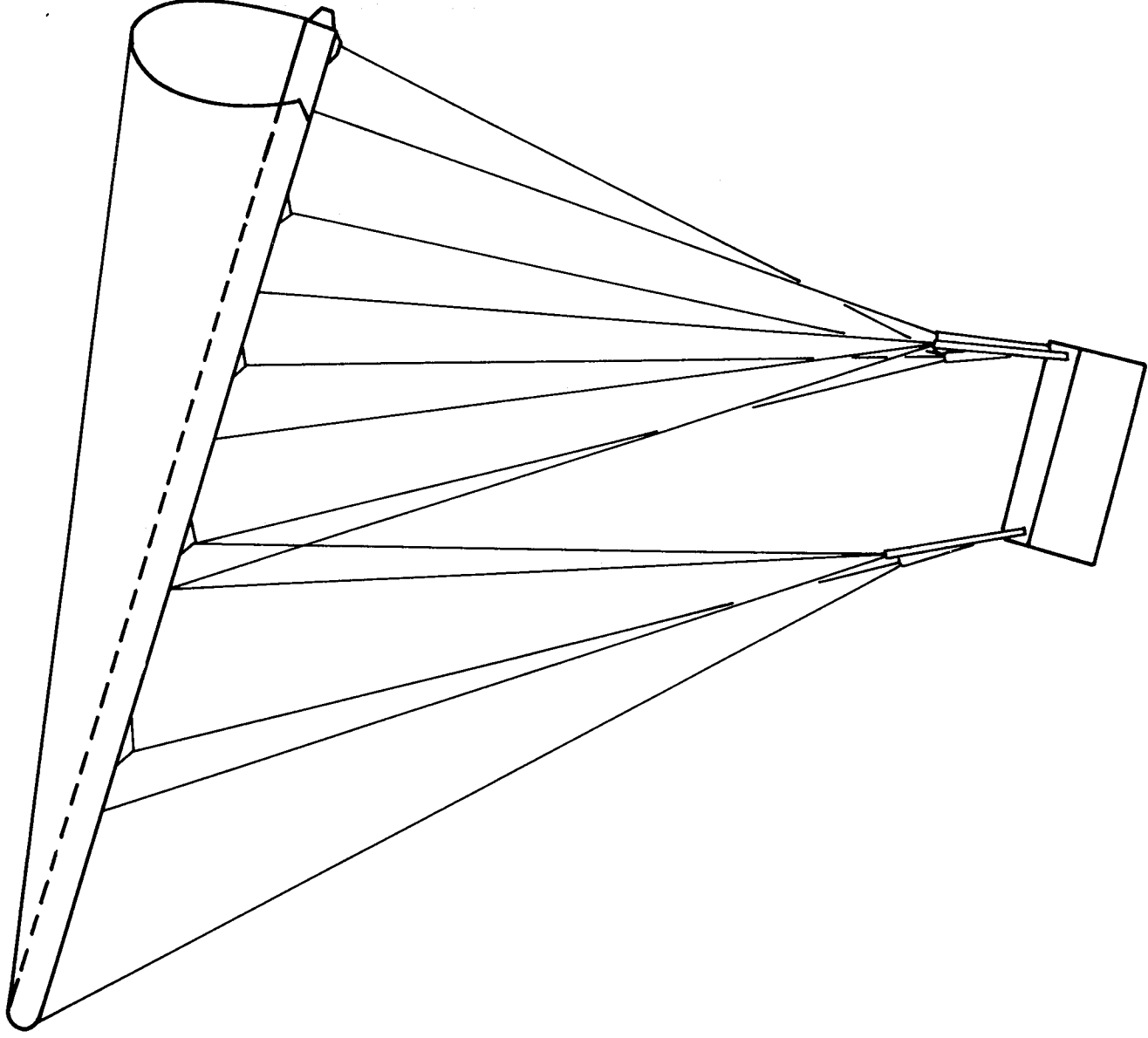
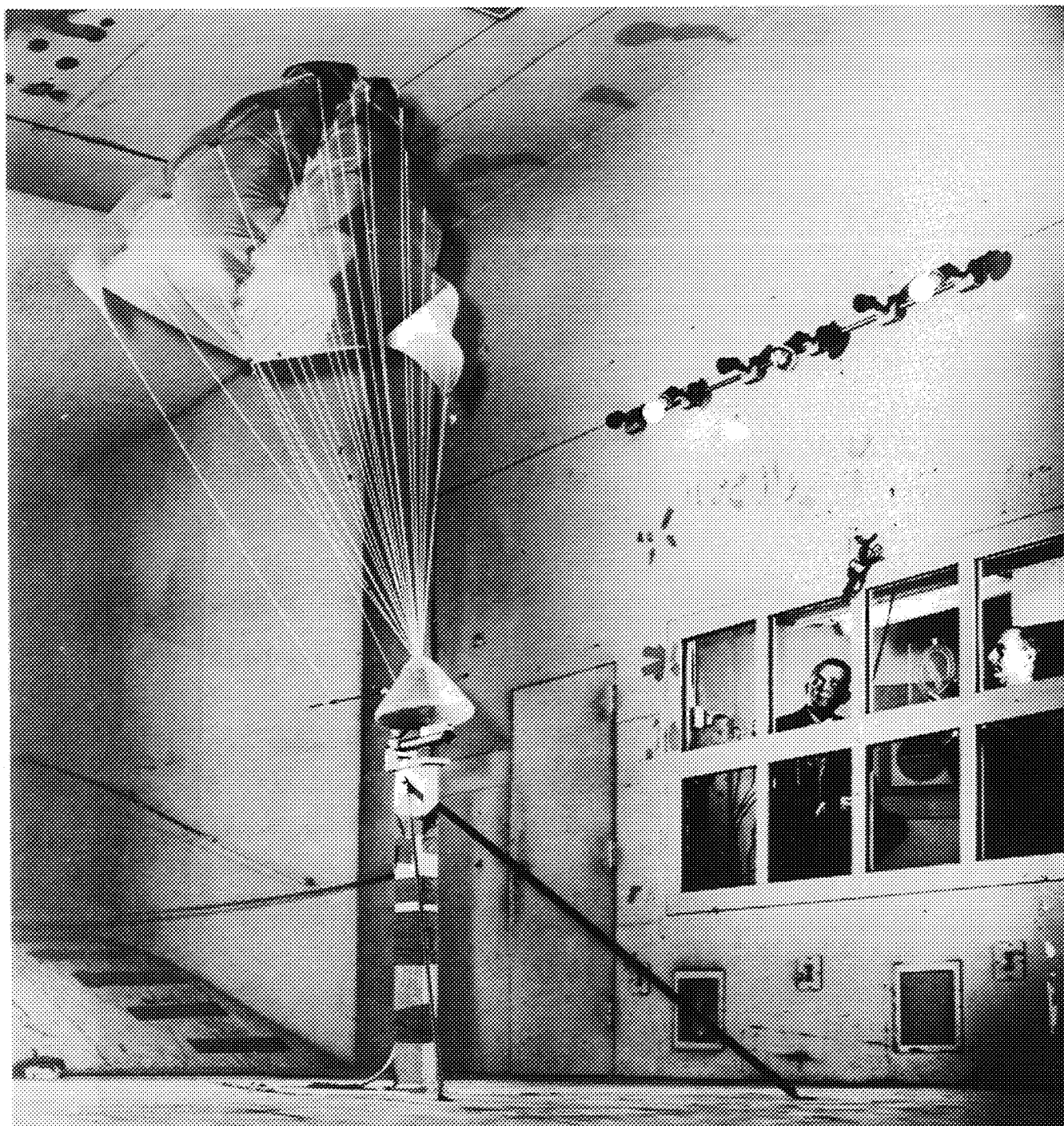
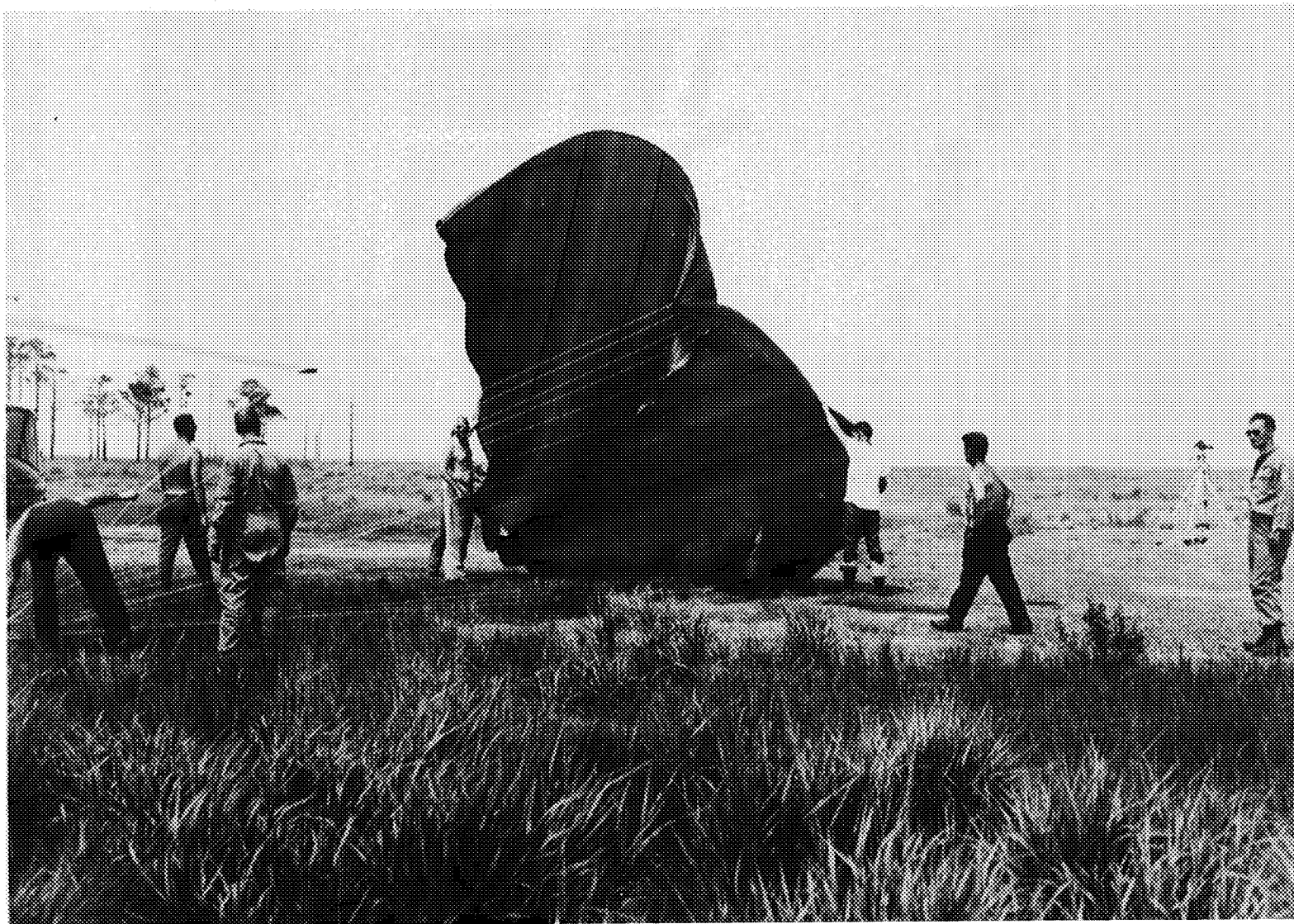


Figure 8.- U.S. Army Precision Drop Glider.



L-65-2412

Figure 9.- Wing-type gliding parachute (limp paraglider) tested in the 17-foot test section of the Langley 300-mph 7- by 10-foot tunnel.



L-65-4993

Figure 10.- Photograph of 24-foot limp paraglider before repacking.



L-65-5196

Figure 11.- Method of folding 24-foot limp paraglider for repacking.

Figure 12.- Photograph of packaged 24-foot paraslider and 500-pound payload on the cargo hook of the UH-1 helicopter.

I-65-5195



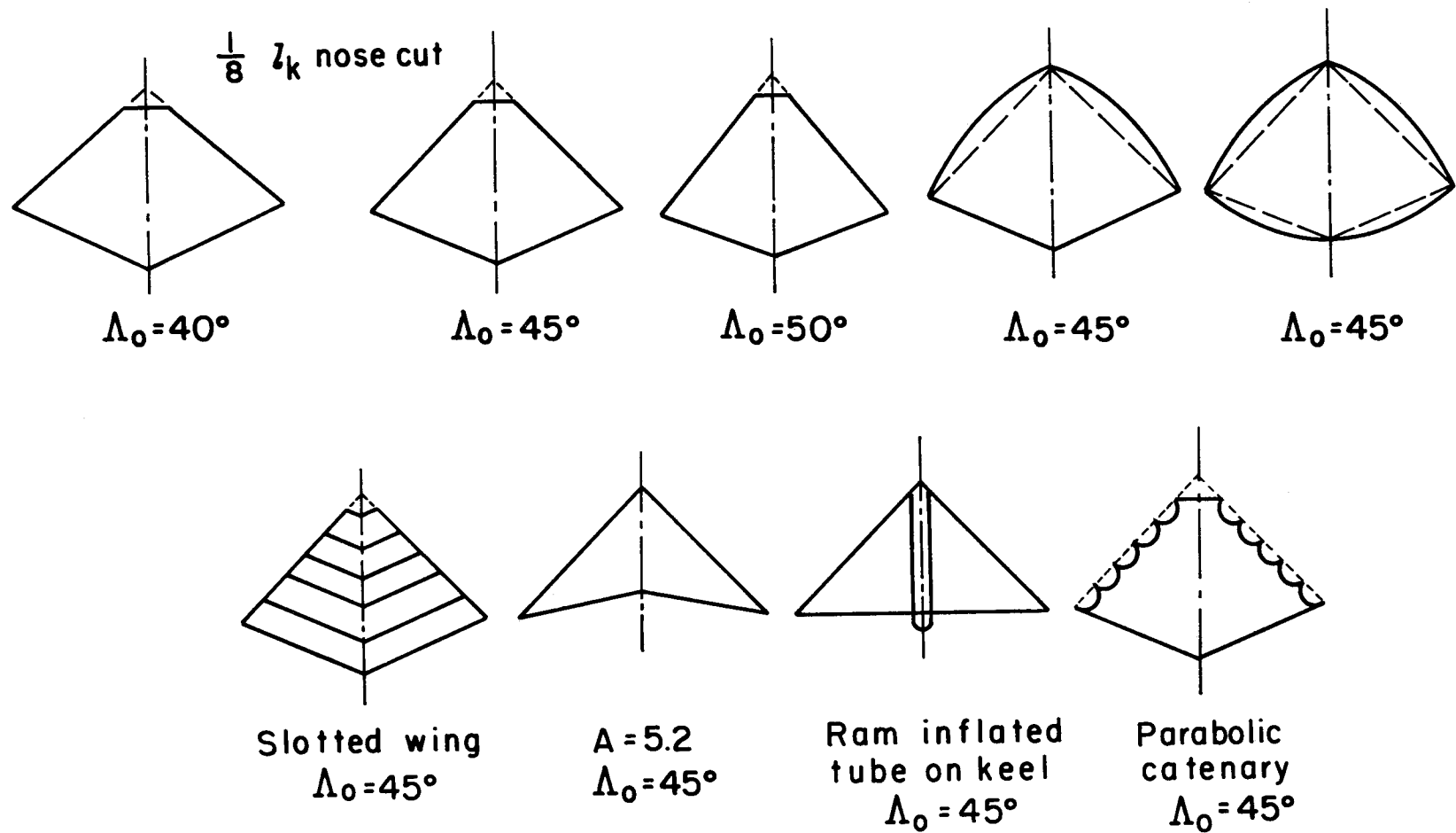


Figure 13.- Wing-planform variations of canopy flat patterns studied in wind-tunnel and flight tests of limp paragliders.

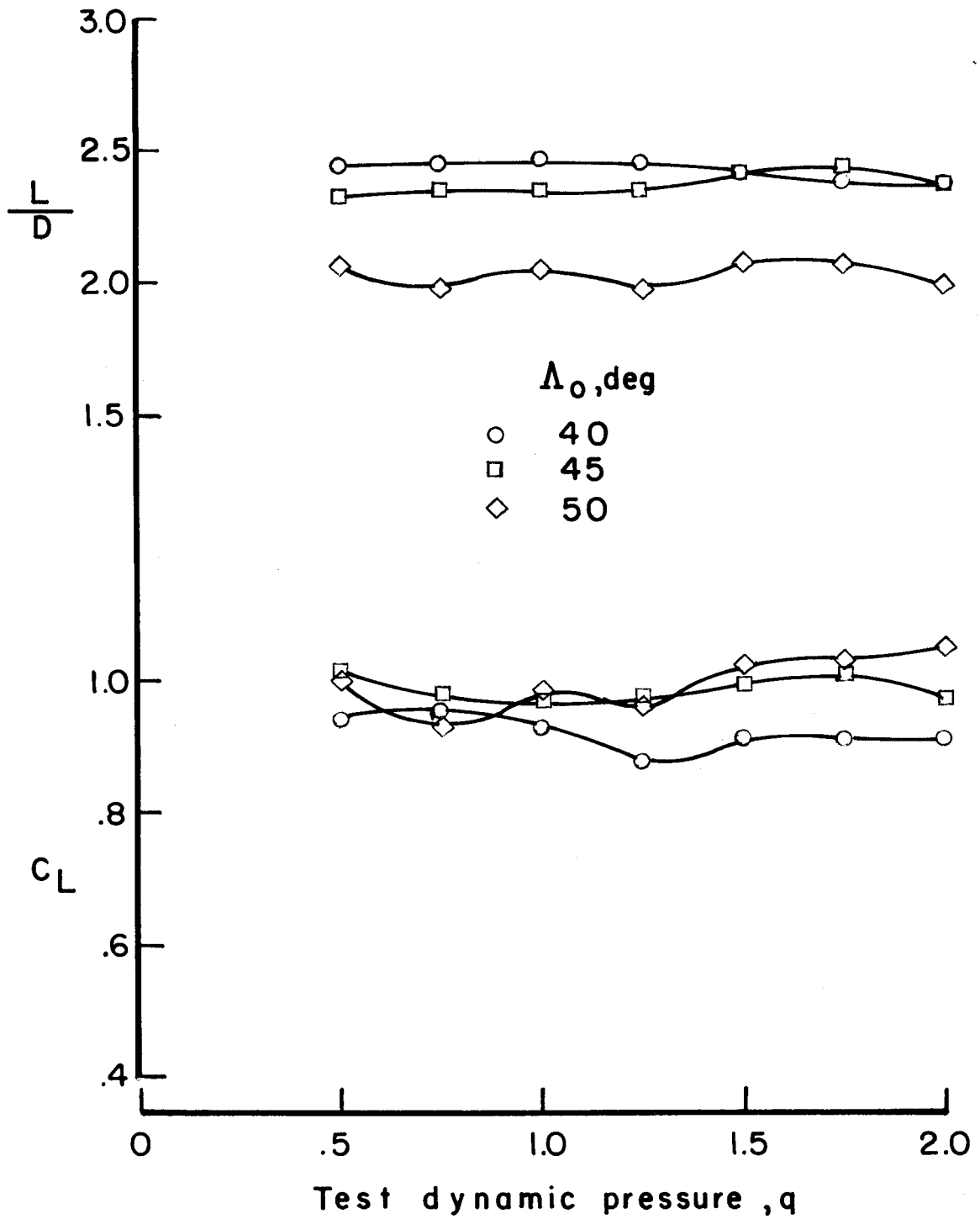


Figure 14.- Effect of canopy flat pattern sweep on lift-drag ratios of 5-foot limp paragliders having  $\frac{1}{8}l_k$  nose cut and nylon lines.

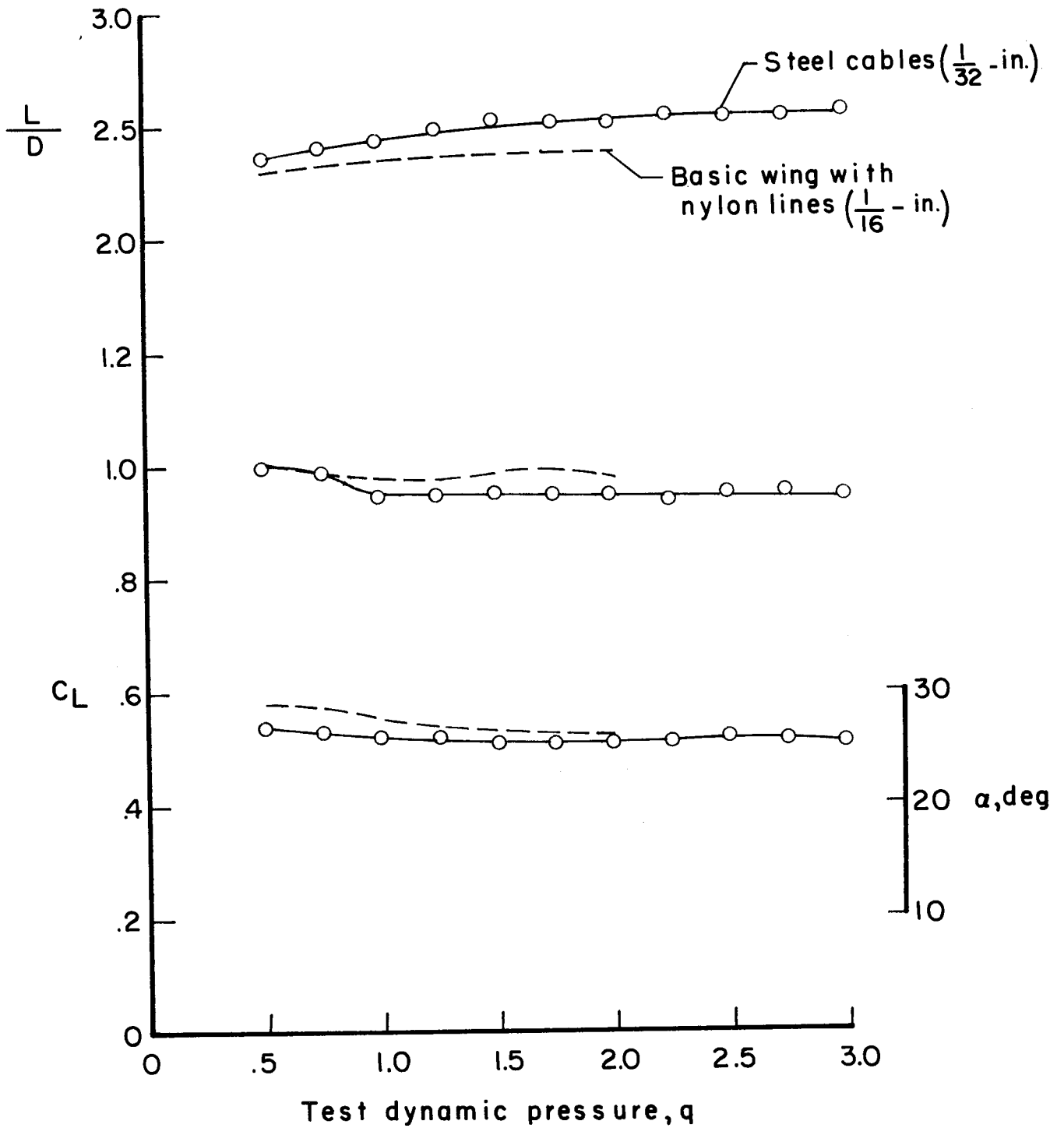


Figure 15.- Comparison of data on  $45^\circ$  swept limp paraglider as obtained with steel cables and nylon lines.

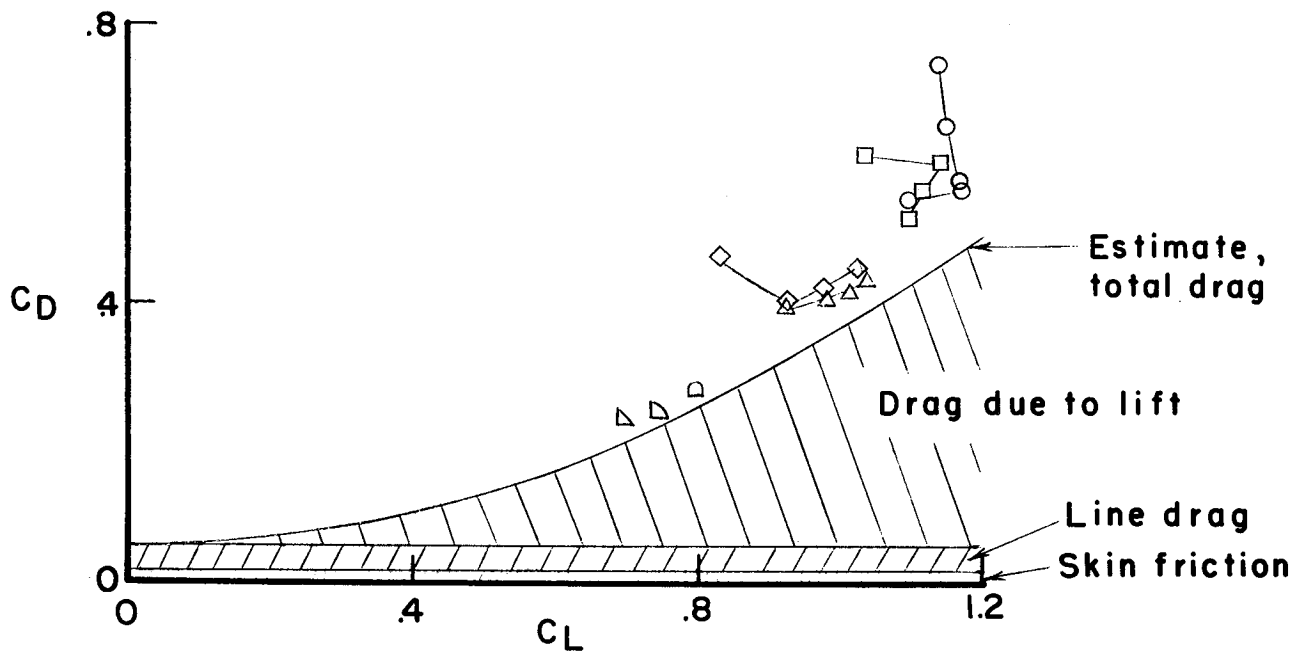
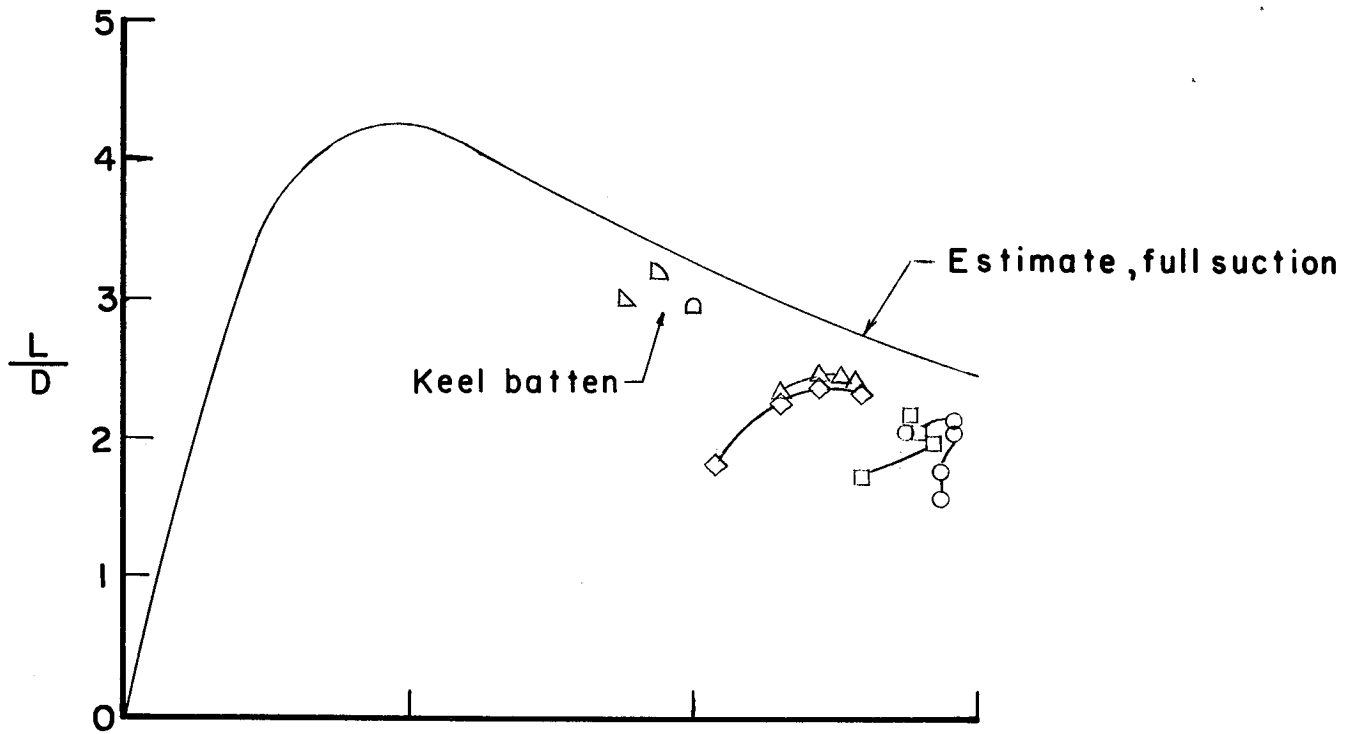


Figure 16.- Comparison of experimental and estimated drag and lift-drag ratios for 5-foot limp paragliders with  $\frac{1}{8}l_k$  nose cut and nylon lines.

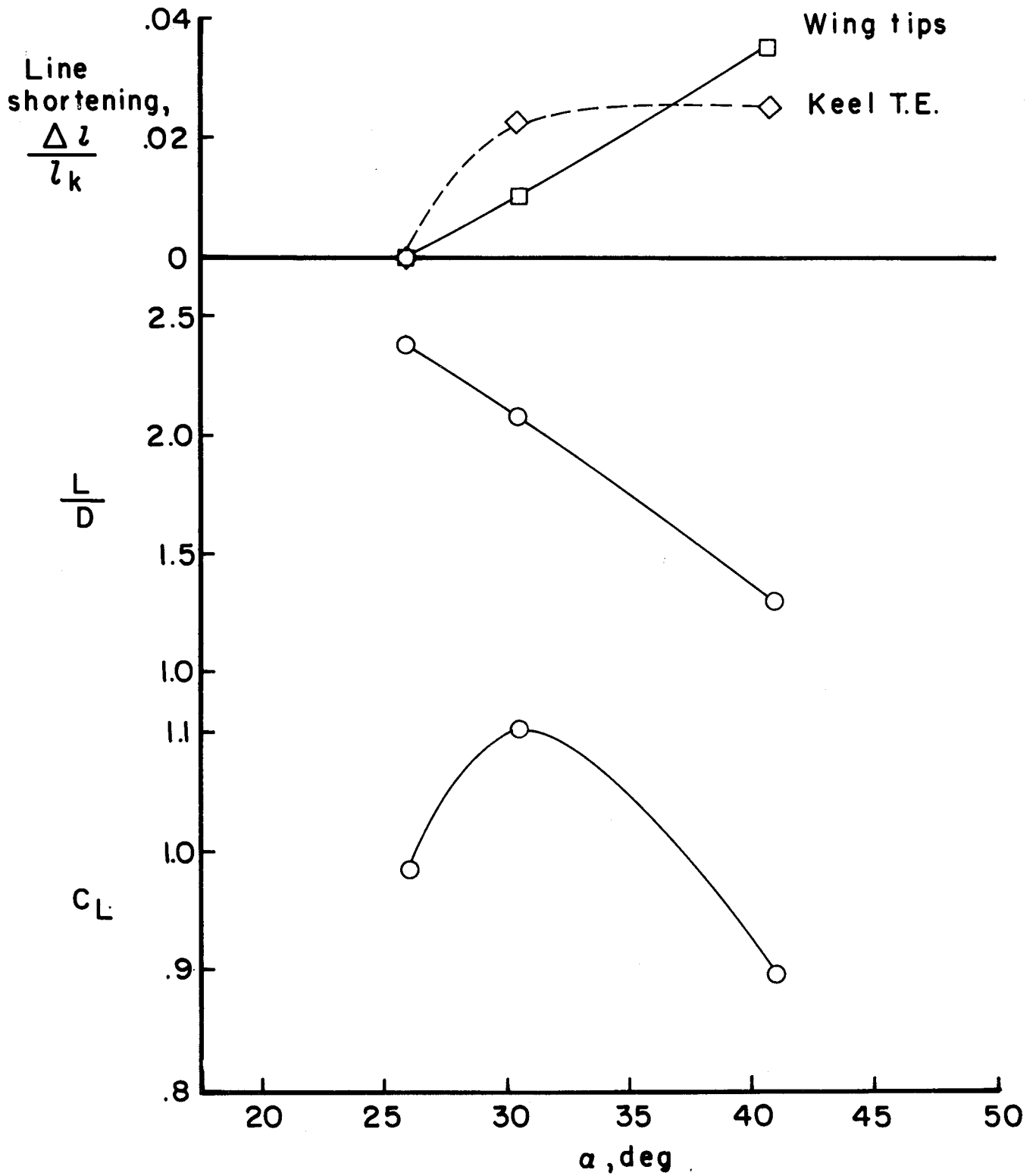


Figure 17.- Modulation of  $C_L$  and  $L/D$  by rigging changes on a  $45^\circ$  swept 5-foot limp paraglider with  $\frac{1}{8}l_k$  nose cut.

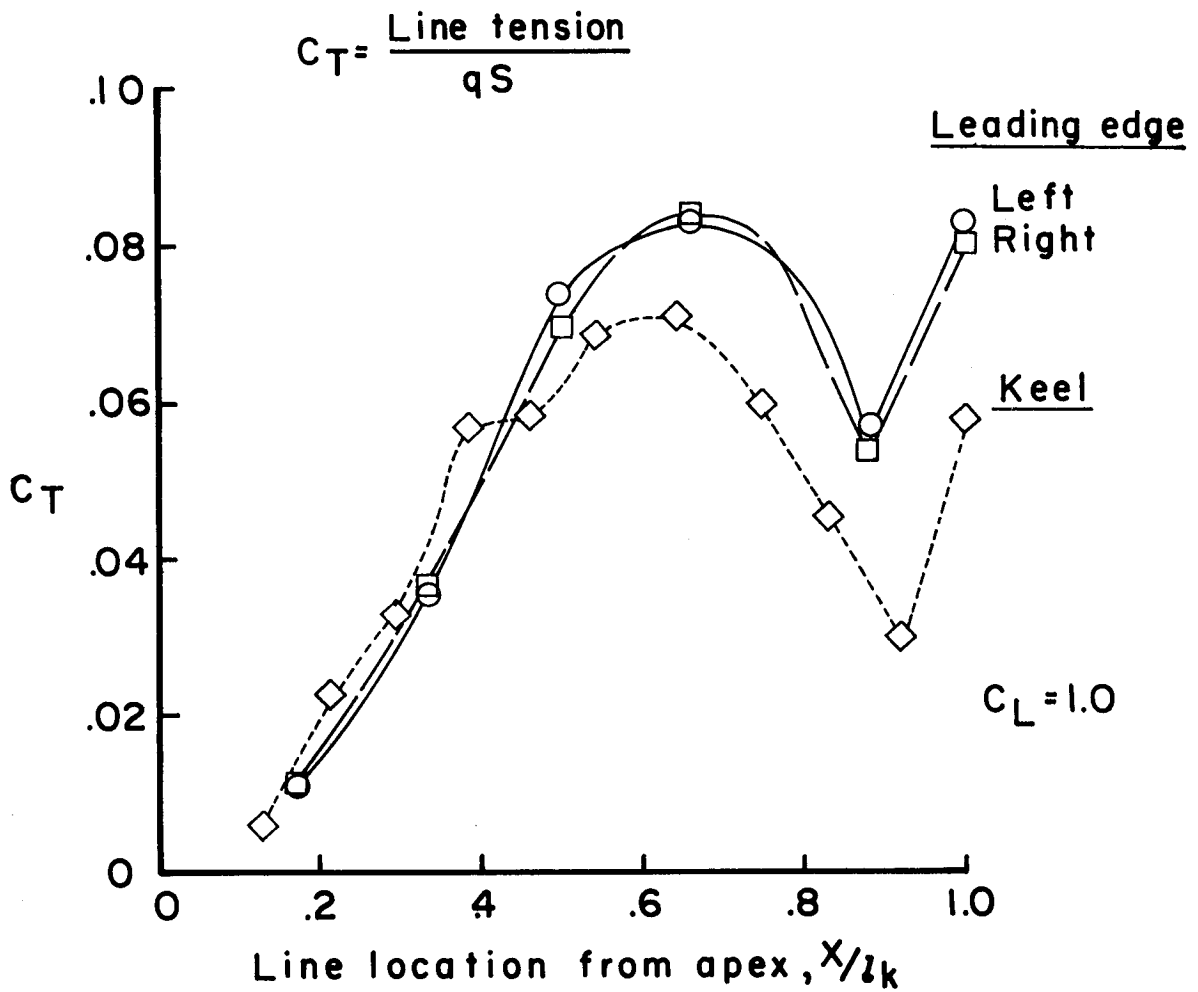
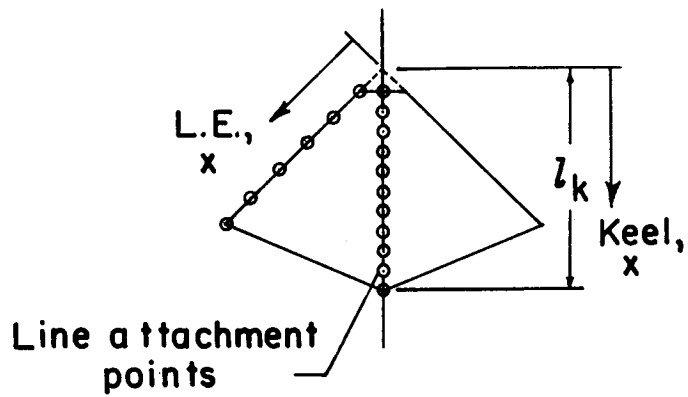


Figure 18.- Line-tension coefficients for  $45^\circ$  swept 5-foot limp para-glider with  $\frac{1}{8}l_k$  nose cut and nylon lines.

- Right tip line shortened
- Differential control of left and right tip lines

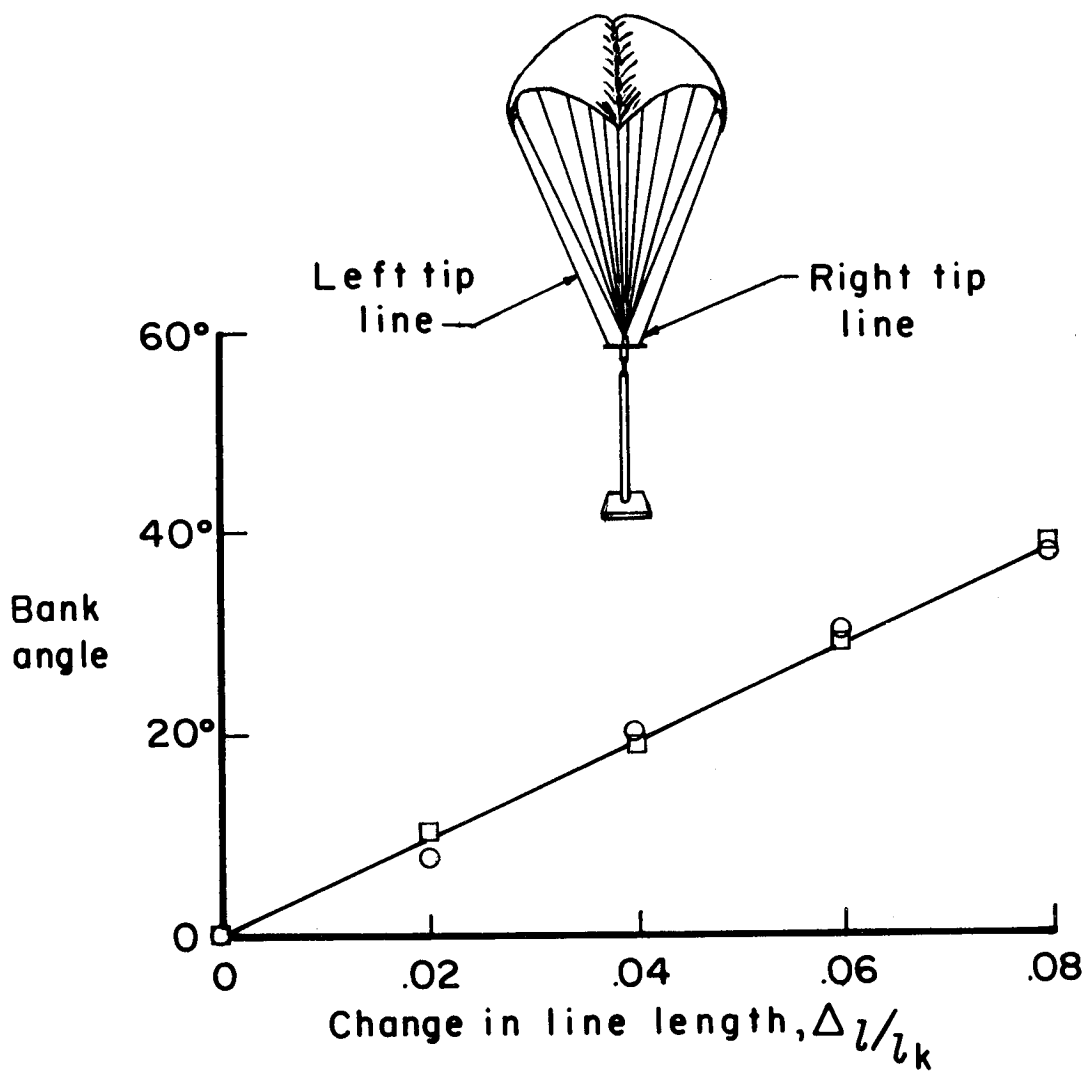


Figure 19.- Roll control by changing the length of the tip lines on a 45° swept 5-foot limp paraglider with  $\frac{1}{8}l_k$  nose cut.

Free drop test from Cherry Picker  
Velocity at wing filling approx. 50 fps  
Weight = 16.86 lbs

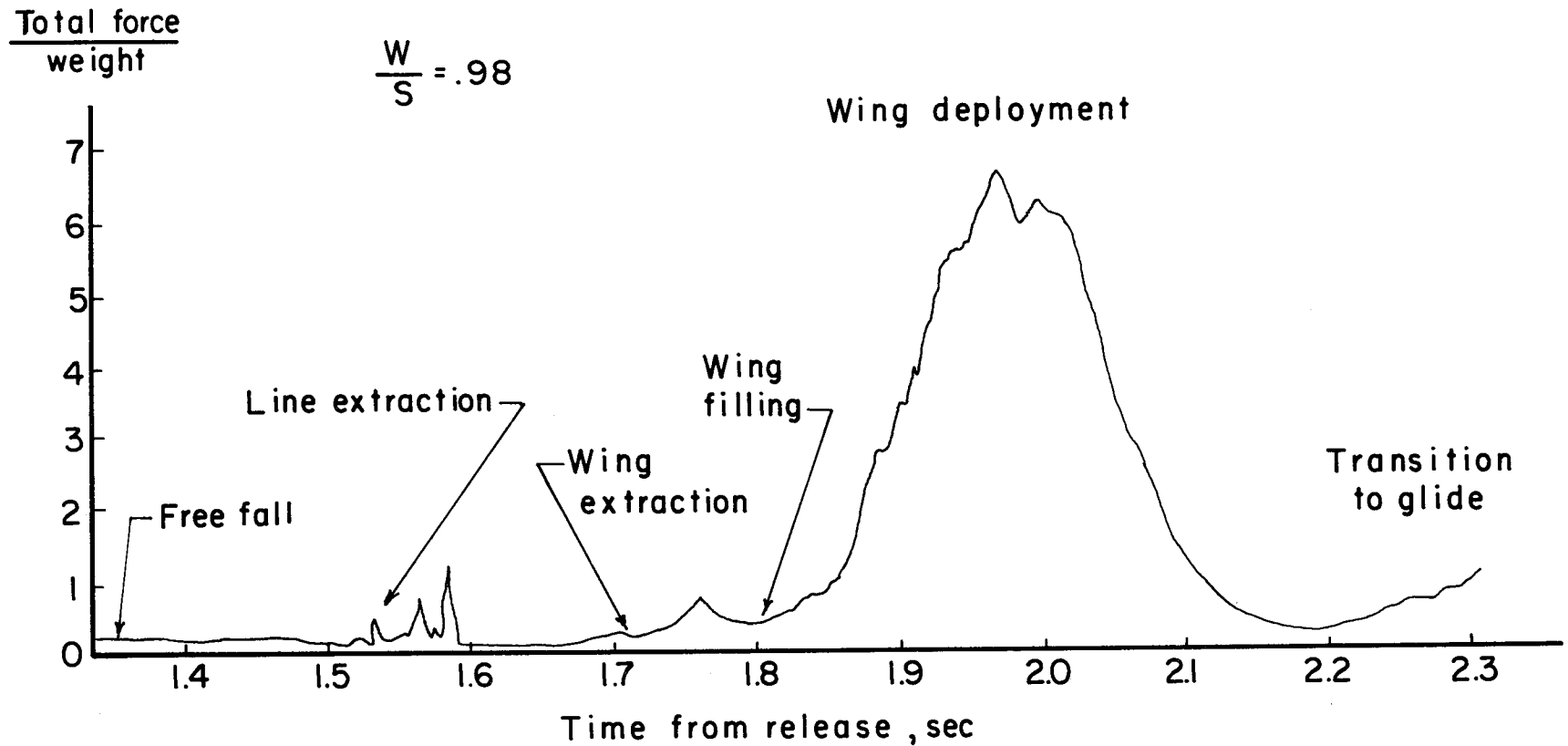


Figure 20.- Time history of total load during deployment of  $45^\circ$  swept 5-foot limp paraglider with  $\frac{1}{8}l_k$  nose cut.

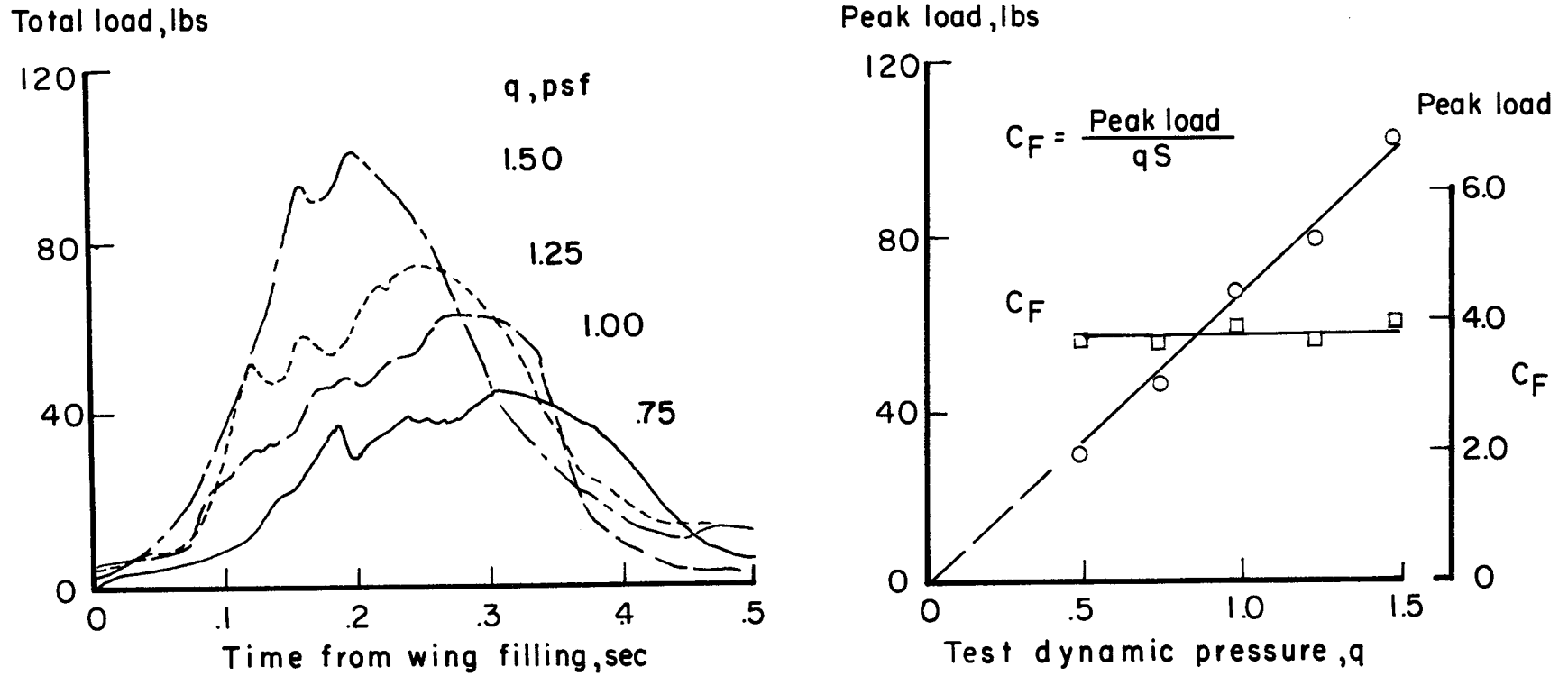


Figure 21.- Data obtained in wind-tunnel deployments of a  $45^\circ$  swept 5-foot limp paraglider with  $\frac{1}{8}l_k$  nose cut.